Hybrid Advances 10 (2025) 100479

Contents lists available at ScienceDirect

Hybrid Advances

journal homepage: www.journals.elsevier.com/hybrid-advances

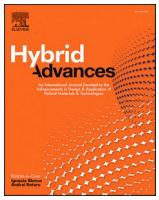

Research Article

Performance of geopolymer mortar incorporating spent coffee grounds as a recycled building material: An experimental and predictive analysis

Ahmet Ferdi Şenol

Bilecik Seyh Edebali University, Faculty of Engineering, Department of Civil Engineering, TR, 11100 Bilecik, Turkiye

ARTICLE INFO

Keywords:
Geopolymer
Spent coffee grounds
Blast furnace slag
High temperature
Multiple linear regression
Microstructure

ABSTRACT

Spent coffee grounds ash (K) is investigated as a sustainable partial sand replacement (0 %, 5 %, 10 %, 15 %) in geopolymer mortars based on granulated blast furnace slag. This study assesses workability, mechanical performance, high-temperature resistance, and microstructure through experimental testing and statistical analysis. Key findings indicate that K content significantly influences workability, strength, and physical properties. Replacing sand with K reduced workability by up to 21 % due to its finer particle size and porosity. The K5 series, containing 5 % K, exhibited the highest compressive strength improvement, with gains of 8.9 % and 16.3 % at 7 and 28 days, respectively, compared to the control. However, higher K contents (10 %, 15 %) negatively impacted mechanical performance. At elevated temperatures, significant mass loss occurred up to 400 °C, after which it stabilized at 600 °C while maintaining structural integrity. Porosity and water absorption increased with K content, except in K5. Microstructural analysis revealed that the K5 series formed a dense, crack-minimal matrix, whereas K10 and K15 exhibited more microcracking and porosity. Statistical models confirmed that temperature had the greatest influence on compressive and flexural strengths, whereas K content significantly affected mass loss.

1. Introduction

The global population and urbanization rates are increasing rapidly. This trend is driving growth in Portland cement production to meet the demands of the concrete industry. Consequently, cement production is consuming greater amounts of energy and generating elevated levels of carbon emissions [1]. To mitigate these effects, researchers are developing cement-free composites. These composites seek to minimize the adverse environmental impacts associated with cement on a global scale. Furthermore, there is a pressing need to investigate green and sustainable alternatives to traditional aggregates. Such alternatives have the potential to reduce environmental degradation and decrease reliance on non-renewable resources.

Geopolymer mortars and concretes offer a sustainable alternative to conventional Portland cement-based materials, exhibiting superior mechanical strength and durability. The primary aluminosilicate precursors for geopolymer production are granulated blast furnace slag (BFS) and fly ash (FA) [2]. Alkaline solutions are commonly employed to activate these materials, with the most widely used activators being sodium hydroxide (NaOH), sodium silicate (Na_2SiO_3), potassium silicate (K_2SiO_3), and potassium hydroxide (KOH) [3]. The hydration products of geopolymers vary depending on the type of activator utilized. When NaOH is applied, the predominant products are sodium-alumino-silicate-hydrate (*N*-A-*S*-H) and calcium-alumino-silicate-hydrate (*C*-A-*S*-H). Conversely, activation with KOH primarily results in the formation of potassium-alumino-silicate-hydrate (K-A-*S*-H) [4].

Rapid urbanization and expanding construction activities have heightened the demand for natural aggregates, which constitute approximately 70–80 % of the total volume of concrete. To address this challenge, researchers are investigating the use of waste and recycled aggregates as viable alternatives. These materials not only improve the economic viability and durability of mortar and concrete production but also contribute to the conservation of natural aggregate resources [5].

Granulated blast furnace slag (BFS) is an industrial byproduct primarily composed of calcium, silica, and alumina. It is generated as a secondary product during iron manufacturing in blast furnaces. In the steel production process, approximately 340–421 kg of blast furnace slag is produced per ton of steel. Currently, only a minor fraction of this waste is repurposed, with the majority being disposed of in landfills. Nevertheless, incorporating BFS as a substitute for cement in geopolymer mortars and concrete significantly reduces CO_2 emissions [6,7]. In recent years, numerous studies have investigated the

E-mail address: ahmetferdi.senol@bilecik.edu.tr.

https://doi.org/10.1016/j.hybadv.2025.100479
Received 3 December 2024; Received in revised form 21 March 2025; Accepted 4 April 2025
Available online 4 April 2025

high-temperature resistance of geopolymer composites derived from waste materials [8–12]. Although Portland cement concrete (PCC) is a widely utilized construction material, it undergoes irreversible degradation when exposed to elevated temperatures. Geopolymers, first developed by Davidovits in 1978, exhibit superior fire resistance and enhanced mechanical properties at high temperatures compared to PCC [13]. In a study by Chithambaram S. et al. [12], researchers investigated geopolymer mortar samples in which fly ash-based geopolymer mortars were partially substituted with up to 30 % blast furnace slag. Various molarities of alkaline activators were employed during the preparation process. The study assessed the impact of high temperatures, ranging from 200 °C to 1000 °C, on the hardened mortar samples following 28 days of ambient curing. The findings revealed that the compressive strength of the geopolymer mortars decreased as the temperature increased, accompanied by a corresponding increase in weight loss under these conditions.

Coffee is the second most consumed beverage worldwide, after tea. In many countries, spent coffee grounds (SCG), classified as agricultural waste, are commonly disposed of in landfills. Owing to their composition, which includes approximately 15 % lipid content, SCG exhibit a higher calorific value than woody biomass, rendering them an abundant and cost-effective renewable energy resource suitable for biofuel production [14]. However, biogas generation from SCG is considered environmentally unsustainable due to concerns regarding toxicity and air pollution. Furthermore, landfilling SCG poses substantial environmental risks, as leachate from these grounds can contaminate water sources, potentially causing eutrophication and excessive algal growth, both of which degrade water quality [15]. Additionally, the disposal of SCG in landfills presents economic and environmental challenges, primarily due to methane emissions produced during decomposition, which contribute to the accumulation of greenhouse gases [16].

A review of the literature reveals that numerous recent studies have explored the use of SCG in developing innovative recycled construction materials. SCG, characterized by its sand-like particle size, low thermal conductivity, and porous structure, is recognized as a sustainable bio-aggregate and is proposed as an alternative to sand in construction applications [17]. However, due to its high organic content, SCG requires specific preprocessing treatments before it can be effectively utilized as a construction material [18]. The combustion of SCG in a furnace demands significant energy due to the requirement for sustained, controlled heating over extended periods. Conventional thermal treatment of SCG typically involves electrically heated furnaces, where the material is subjected to temperatures between 350 °C and 650 °C for 1–2 h to facilitate the decomposition of organic matter and its conversion into biochar [19,20]. This process relies on a continuous external energy supply, resulting in substantially elevated energy consumption and operational costs. In contrast, this study employed a self-combustion technique, incinerating SCG in a controlled, oxygen-rich open-air environment without additional energy input. This method capitalized on SCG's low auto-ignition temperature of approximately 169 °C [21], enabling self-sustained combustion following ignition. Furthermore, with a composition that includes approximately 15 % lipid content, SCG exhibits a calorific value surpassing that of many woody biomass sources, promoting efficient energy release during combustion [19]. Consequently, this approach proved more economical and energy-efficient than traditional furnace-based combustion, which necessitates constant heating and meticulous process oversight. Additionally, the heat generated during open-air combustion could potentially be captured for secondary applications, such as preheating raw materials or supplementing industrial drying processes, thereby enhancing overall energy utilization compared to furnace combustion, where a significant portion of the heat is lost to the environment. While open-air incineration may raise concerns about emissions, the controlled conditions applied in this study—such as the use of thin SCG layers to optimize oxygen availability—effectively minimized incomplete combustion and associated pollutant emissions. Moreover, compared to alternative disposal methods for SCG, such as composting or direct land application, the incineration technique adopted here offers a practical approach to SCG valorization, simultaneously reducing waste volume and generating valuable byproducts. Nevertheless, incorporating the ash derived from the complete incineration of dried SCG as a fine aggregate replacement in geopolymer mortars can effectively fill voids through pore-filling mechanisms, increase packing density, and enhance the microstructural integrity of the matrix.

According to Garcia et al. [21], the presence of oils and lipids in spent coffee grounds (SCG), constituting 11 %–15 % by weight, enables incineration at a relatively low ignition temperature of 169 °C. The integration of SCG ash into geopolymer mortars post-incineration may affect the matrix's strength, density, and durability properties. Mohamed and Djamila [22], explored the use of SCG as a fine aggregate in concrete production. In their study, sand was partially substituted with SCG at volumetric ratios of 5 %, 10 %, 15 %, and 20 %. The results revealed that replacing natural sand with SCG increased porosity, leading to decreased workability, unit weight, and mechanical strength in the concrete mixtures. However, thermal properties were enhanced, particularly at replacement levels of 15 % and 20 %. Lawanwadeekul et al. [23] examined the incorporation of SCG and waste glass (WG) as additives to enhance the properties of clay bricks fired at low temperatures. Their results showed that adding 10 % SCG and 10 % WG to clay mixtures and firing at 950 °C improved strength, porosity, and thermal conductivity while adhering to required standards, thus supporting sustainable brick production. In a separate study, Roychand et al. [19], investigated SCG as a partial substitute for fine aggregate in concrete mixtures at volumetric ratios of 5 %, 10 %, 15 %, and 20 %. Three SCG variants were employed: raw SCG and SCG pyrolyzed at 350 °C and 500 °C. The findings revealed that pyrolysis of SCG at 350 °C markedly improved material properties, resulting in a 29.3 % increase in the compressive strength of the composite concrete. Arulrajah et al. [18] developed geopolymer mortar samples by activating mixtures of sugarcane bagasse ash, SCG, and slag with a sodium hydroxide (NaOH) solution. The samples were cured at 21 °C and 50 °C, with the highest compressive strength (1.48 MPa) recorded in a mixture comprising 70 % SCG, 20 % sugarcane bagasse ash, and 10 % slag after 90 days of curing at 50 °C. In a separate study, Giada La Scalia et al. [24] evaluated the technical, environmental, and economic performance of SCG in natural hydraulic lime and geopolymer-based mortars. Their results indicated that the incorporation of SCG increased water absorption while improving insulation performance. Specifically, adding SCG at a 5 % ratio significantly lowered thermal conductivity, thereby enhancing the insulating properties of the mortars. Saeli et al. [25] developed eco-friendly bio-composite mortars by partially substituting sand with SCG. The SCG content was incrementally increased to a maximum of 15 % and evaluated using various binder combinations, such as Portland cement and natural hydraulic lime. The findings indicated that the incorporation of SCG improved the insulation properties of the mortars, achieving a thermal conductivity reduction of up to 72 %, while also lowering costs by as much as 8 % and preserving satisfactory mechanical performance.

Numerous researchers have analyzed the chemical composition of SCG and its potential as a mineral admixture or aggregate in cementitious composites. However, investigations into its effects on the physical and mechanical properties of geopolymer mortars and concretes remain comparatively scarce. Although the incorporation of SCG into geopolymer mortars is not a novel concept, research exploring the properties of geopolymer mortars formulated with SCG and BFS is still in its preliminary stages. This study aims to assess the feasibility of utilizing spent coffee grounds ash (SCG ash), denoted as K, obtained from the incineration of SCG sourced from local cafeterias, as a sand replacement in the production of BFS-based geopolymer mortars. Specifically, it investigates the influence of K, derived through a process that requires no additional energy input or high costs, on the development of sustainable construction materials. In this context, the study seeks to promote SCG

valorization while mitigating its environmental footprint in the construction sector. To achieve this, geopolymer mortar series were produced by replacing sand with 5 %, 10 %, and 15 % K. Additionally, a control series (C) containing only BFS was prepared to evaluate the workability, physical, and mechanical properties, as well as the high-temperature resistance and microstructural characteristics of all series. The study further examines the effects of K content (%) as a sand substitute and the influence of elevated temperature (T) on the performance of BFS-based geopolymers. The evaluation of workability (F), compressive strength (CS), flexural strength (FS), and mass loss (M) in the produced mortar series is conducted using multiple regression models and Pearson correlation analysis. Ultimately, this study aims to determine the optimal replacement levels of K in geopolymer mortars, contributing to the economic valorization of SCG and the development of lightweight, sustainable geopolymer mortars.

2. Materials and methods

2.1. Materials

The SCG utilized in the study was procured from local cafeterias and initially subjected to oven drying at 70 °C for approximately 24 h until a constant weight was attained, thereby ensuring the removal of moisture. The collected SCG had a maximum particle size of 1 mm and a specific gravity of 0.47 (Fig. 1). Additionally, the water absorption capacity of SCG by weight was determined to be 122 %. As observed in the FESEM analysis shown in Fig. 1, the SCG particles exhibited angular shapes and possessed numerous pores on their rough, corrugated surfaces [26,27].

Due to the high organic content of SCG in its natural state, incineration was permitted to occur in an open-air environment, which was oxygen-rich, without the necessity for additional energy input. This resulted in the complete conversion of SCG to ash (K), which was then used in the production of geopolymer mortar (Fig. 2).

The incineration of SCG was conducted in an open-air environment. During combustion, the surface temperature of the material was monitored periodically using a thermal camera and ranged between 250 °C and 300 °C. After approximately 30 min, the combustion naturally ceased, and the temperature gradually declined as the material cooled. The specific gravity of the resulting ash (K) was measured as 0.22. The specific gravity of the dry SCG was observed to decrease by 53 % as a consequence of incineration. The granulated blast furnace slag (BFS), employed as an aluminosilicate source in the geopolymer mortar mixtures, was procured from local iron and steel plants and utilized without any additional processing (specific gravity: 2.9). In order to prevent any secondary effects of potential impurities in natural sand on the

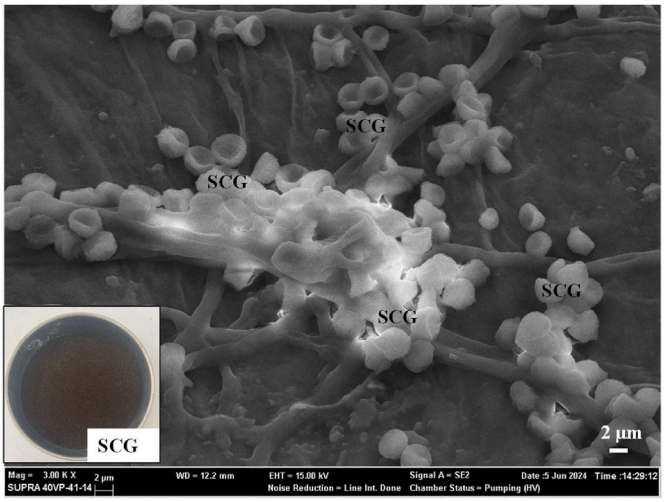

Fig. 1. FESEM micrograph (×3000 magnification) of SCG.

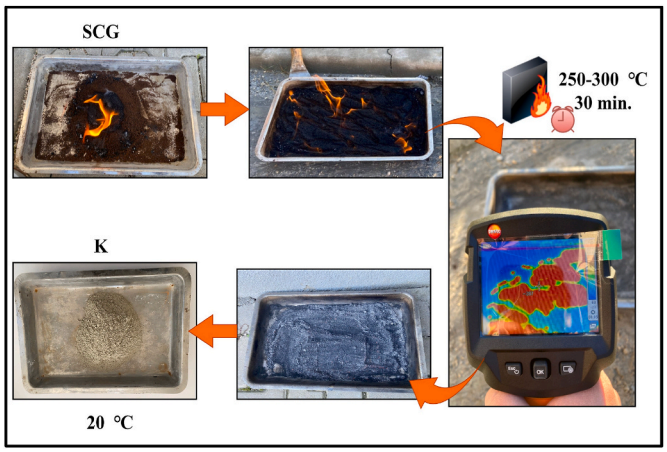

Fig. 2. Ash (K) obtained after the incineration of SCG.

geopolymer matrix, CEN standard sand, which conforms to TS EN 196–1 [28], was sourced locally and used in the production of mortar series. The CEN standard sand, with a specific gravity of 2.56 and a water absorption rate of 0.63 %, has a particle size range of 0–2 mm. The sand is composed of rounded grains derived from natural silica sand, with a minimum SiO_2 content of 98 %. The dry bulk density of the sand used in the mixtures was 1480 kg/m^3, whereas that of K was 145 kg/m^3, reflecting the significant density contrast that supports the volume-based replacement approach in the mix design. Fig. 3 illustrates the particle size distributions of sand, K and BFS. As illustrated in Fig. 3, the mean diameter of K is approximately 30 µm, the BFS is 11.4 µm, and the sand is 800 µm. The results of the chemical analysis of the BFS, K, and sand employed in the mixtures are presented in Table 1. As illustrated in Table 1, the primary chemical constituent of BFS is calcium oxide (CaO), whereas that of K is potassium oxide (K_2O). K exhibits a high Loss on Ignition (LOI) value (33.65 %) due to its substantial content of organic compounds, including fatty acids, amino acids, polyphenols, and polysaccharides [29,30]. A high LOI may elevate the water demand of the mortar, influencing its fresh and hardened properties by promoting microvoid formation due to the gradual release of volatile components during curing. The surface texture and particle shape of the K and BFS used in the mortar series were observed using a Zeiss LEO 1430 V P field emission scanning electron microscope (FESEM) (Fig. 4). The FESEM analysis revealed that the structure of K is irregular and angular, with surfaces composed of corrugated and rough particles

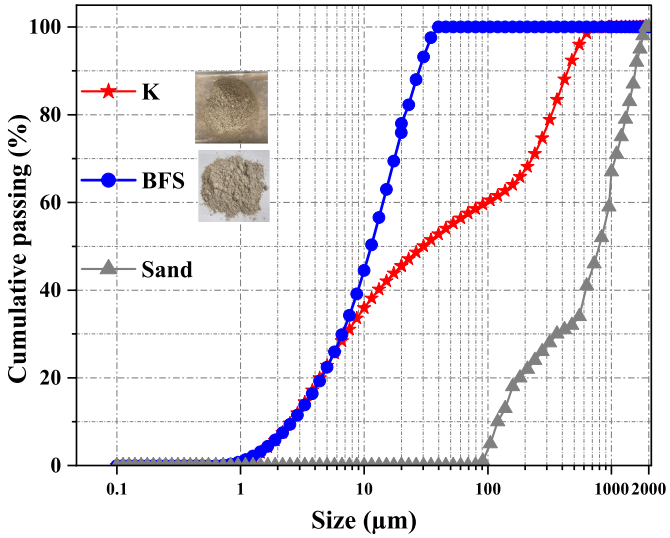

Fig. 3. Particle size distribution curves of powder materials and sand.

Table 1
Chemical properties of powder materials.

Oxides components, %	K	BFS	Sand
SiO_2	1.45	32.1	98.8
Al_2O_3	0.70	11.2	0.05
Fe_2O_3	0.98	0.62	0.02
CaO	12.35	36.1	0.01
MgO	7.52	5.6	0.03
SO_3	1.25	1.2	–
K_2O	35.45	0.83	–
Loss of ignition	33.65	2.35	–

(Fig. 4(a)). As illustrated in Fig. 4(b), the BFS particles exhibit an irregular and sharp-edged surface. In comparison to the K particles, the BFS particles display a more uniform and less irregular surface. The production of the geopolymer mortar series utilized tap water as the mixing water.

The NaOH (98 % purity) was procured from Lapointe Co. Ltd., while the Na_2SiO_3 (99 % purity, specific gravity; 1.4 and 3 module) was obtained from Detsan Co. Ltd. These alkaline solutions were subsequently employed in the preparation of the mixtures. The Na_2SiO_3 solution consists of approximately 36 % solids and 64 % liquid (H_2O) materials.

2.2. Methods

2.2.1. Mixture proportions

In the geopolymer mortar mixtures, K partially replaced sand at levels of 5 %, 10 %, and 15 % by volume, owing to its low specific gravity (0.22) compared to sand (2.56). With a water absorption capacity of 5.44 % by weight (versus 0.56 % by weight for sand), determined prior to mixing, K was in a dry state due to the incineration process, exhibiting minimal bulking that did not significantly affect the mix proportions, as confirmed by visual inspection and physical handling during preparation. Accordingly, no additional water was added beyond the specified liquid content, which consisted solely of water from the NaOH and Na_2SiO_3 solutions as detailed in the mixing procedure. No superplasticizers or chemical admixtures were used, with workability managed entirely through the prescribed mix proportions and the inherent properties of the raw materials, enabling an evaluation of K's impact on the fresh properties of geopolymer mortar mixtures. The geopolymer mortar series and their respective mix proportions are presented in Table 2. In the naming of the geopolymer mortar series, the 'K' index indicates the K used as a replacement for sand, while the numerical values represent the volumetric percentage of the material within the total sand volume. For example, the designation K5 refers to a geopolymer mortar mixture in which an amount equivalent to 5 % of the total sand volume is replaced with K.

In the study, preliminary casts were conducted based on similar studies [31–35] to determine the aggregate/precursor ratio and Na_2SiO_3/NaOH ratio for BFS-based geopolymer mortars. For this purpose, mortar series were produced using 10 and 12.5 M (M) NaOH solutions, with an aggregate/precursor ratio of 1.75 and 2, and Na_2SiO_3/NaOH ratios by weight of 1.5 and 2. After 28 days of ambient curing, the compressive strengths of the geopolymer mortar series were measured and the results were evaluated. Based on the curing and mechanical tests, it was determined that the optimal mix design includes a NaOH molarity of 10 M, an aggregate/precursor ratio of 1.75, and a Na_2SiO_3/NaOH ratio of 2.0.

2.2.2. Mixture preparation

In the geopolymer mortar series, the aggregate/precursor ratio by weight was maintained at 1.75, the Na_2SiO_3/NaOH ratio at 2.0, the NaOH solution at 10 M, and the water-to-aluminosilicate source material ratio at 0.32. Before production, the 10 M NaOH solution was stored in glass jars at room temperature for 24 h and mixed shortly before use. In the first stage of producing the geopolymer mortar series, BFS and sand were mixed in a mortar mixer at low speed (62.5 rpm) for 2.5 min. Then, the 10 M NaOH solution was added to the mixer, and mixing continued at the same speed for another 60 s. In the third stage, Na_2SiO_3 was added to the mixture, and mixing continued at low speed for an additional 60 s. Finally, the mortar mixer was set to high speed (125 rpm) for a further 60 s of mixing.

2.2.3. Specimen preparation, curing and testing

The prepared mixtures were placed in 40 mm × 40 mm × 160 mm and 50 mm × 50 mm × 50 mm moulds in two stages using a vibration device, in accordance with the requirements set forth in TS EN 12390–1 [36]. The freshly produced geopolymer mortars were stored in the moulds for the first 24 h in a laboratory environment at a temperature of 20 ± 2 °C. After demoulding, the geopolymer mortar specimens were cured under ambient conditions at 20 ± 2 °C and a relative humidity (RH) of 50 ± 5 % until testing on the 7th or 28th day.

The fresh geopolymer mortar series were subjected to the flow table test according to TS EN 1015–3 [37]. After a specified curing period, tests for unit weight, water absorption, and apparent porosity were conducted according to TS EN 772–4 [38]; ultrasonic pulse velocity

Table 2
Geopolymer mortar series and mix proportions.

Series	NaOH (M)	Na_2SiO_3 (g)	BFS (g)	K (g)	Sand (g)	water/ precursor
C	10	120	700	–	1225	0.32
K5	10	120	700	5.3	1160	0.32
K10	10	120	700	10.6	1100	0.32
K15	10	120	700	15.9	1040	0.32

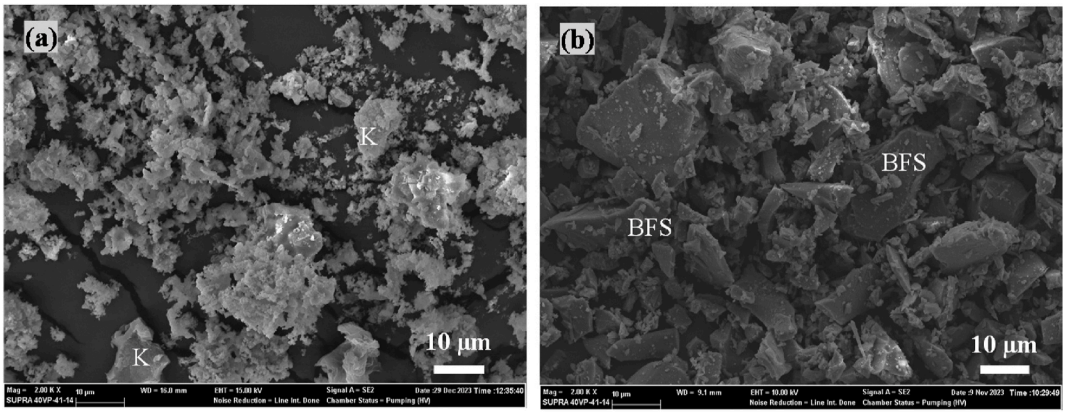

Fig. 4. FESEM micrographs (×2000 magnification) of (a) K, (b) BFS.

testing was performed according to TS EN 12504–4 [39]; and mechanical property tests were carried out according to TS EN 1015–11 [40]. Unit weight, ultrasonic pulse velocity, and flexural strength tests, as well as mass loss and residual flexural strength tests after high-temperature exposure, were conducted on 12 beam specimens of 40 mm × 40 mm × 160 mm for each series. Compressive strength tests before and after high-temperature exposure were conducted on 12 specimens of 50 mm × 50 mm × 50 mm for each series. Apparent porosity and water absorption tests were conducted on three prismatic beam specimens (40 mm × 40 mm × 160 mm) from each series, following a 28-day curing period. The weight of the specimens in water was determined using an Archimedes balance. In all tests, the average results obtained from the specimens in each series were used.

The apparent porosity (P) and water absorption (WA) were determined utilizing an Archimedes balance, with the calculations performed in accordance with Equations (2.1) and (2.2). Furthermore, error bars were generated based on the standard deviation and mean values obtained from the experimental data, thereby illustrating the variability and reliability of the data distribution.

$$P\ (\%) = \frac{(W_1 - W_0)}{(W_1 - W_2)} \times 100 \tag{2.1}$$

$$WA\ (\%) = \frac{(W_1 - W_0)}{W_0} \times 100 \tag{2.2}$$

In the equation, w_0 represents the dry weight of the specimen (g), w_1 represents the weight of the specimen in water-saturated air (g), and w_2 represents the weight of the specimen in water (g).

2.2.4. Heating process

Following a 28-day ambient curing period, the geopolymer mortar specimens were exposed to elevated temperatures, and subsequent changes in mass loss, flexural strength, and compressive strength were evaluated at ambient temperature. Prior to exposure to elevated temperatures, the specimens were pre-dried at 105 °C for 12 h to reduce the risk of fragmentation due to internal steam pressure, as recommended in previous studies [41–43]. A controlled electric furnace was subsequently utilized. The furnace temperature was raised at an average rate of 5 °C per minute to target temperatures of 200 °C, 400 °C, and 600 °C. Upon reaching each target temperature, it was maintained for 1 h to ensure uniform heat distribution within the specimens and to allow the furnace temperature to equilibrate with the internal core temperature of the specimens (Fig. 5). The geopolymer mortar series were then exposed to these elevated temperatures for 1 h, followed by natural cooling to ambient temperature inside the furnace over 24 h. To assess the mass loss of the prismatic specimens following exposure to high temperatures, the difference between their initial mass prior to exposure and their mass after cooling was calculated and expressed as a percentage. Subsequently, compressive and flexural strength tests were performed on the specimens.

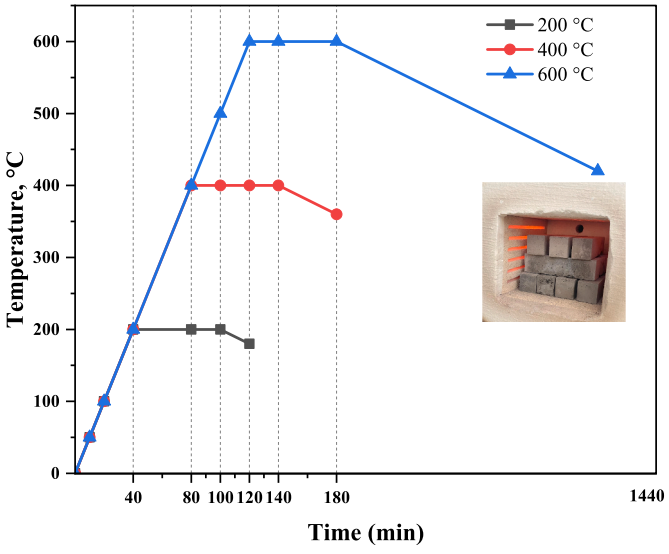

Fig. 5. Experimental heating curve.

Mass loss (M) refers to the change in the mass of the sample before and after exposure to high temperatures, as described in Equation (2.3).

$$M = \frac{m_1 - m_0}{m_0} \tag{2.3}$$

m_1: the mass of the sample after heating (g), m_0: the mass of the sample before heating (at 20 °C, g).

Microstructure analysis was performed on fragments obtained from geopolymer mortar specimens cured for 28 days using a ZEISS Supra 40 V P Field Emission Scanning Electron Microscope (FESEM). The production process and the experimental procedures applied to the geopolymer mortar series in this study are illustrated in the flowchart presented in Fig. 6.

3. Results and discussion

3.1. Workability test results

The flow diameter variations of the geopolymer mortar series are shown in Fig. 7. As indicated in Fig. 7, the flow diameter values for the series ranged from 150 mm to 190 mm. The highest flow diameter was recorded in the C series (190 mm), whereas the lowest was observed in the K15 series (150 mm).

As shown in Fig. 7, the partial replacement of sand with K at specific ratios in geopolymer mortar mixtures significantly affected the fresh-state properties of the mortars. As the proportion of K increased, the flow diameter values decreased. Specifically, the flow diameters of the fresh K5, K10, and K15 mortar series were reduced by 2.6 %, 10.5 %, and 21 %, respectively, compared to the C series. This reduction can be attributed to the irregular, angular shape of K particles, characterized by rough-surfaced grains, as well as their finer particle size relative to sand and higher porosity, which enhances water absorption (see Fig. 4) [44]. The observation that the average diameter of K is approximately 26 times smaller than that of the sand used (Fig. 3) suggests an increased water demand in the mixture, resulting in reduced workability. Furthermore, diminished workability may lead to the formation of a non-homogeneous and poorly compacted matrix, potentially causing a porous structure and subsequent loss of mechanical performance. Additionally, a geopolymer mixture with lower workability could hinder the uniform distribution of particles and binder, possibly resulting in uneven stress distribution under external loads [45]. A similar study [26], reported that replacing up to 17.5 % of sand with SCG in geopolymer mortars caused a significant workability reduction of up to 52 %, attributed to the fine particle size and the organic, porous structure of the material, which enhances water absorption.

3.2. Unit weight and ultrasonic pulse velocity tests results

The unit weights and ultrasonic pulse velocity (UPV) measurement results for the geopolymer series after a 28-day curing period are presented in Fig. 8. The unit weights of the series ranged from 2055 to 2205 kg/m^3. As anticipated, increasing the K replacement level in the mortar series resulted in lower unit weights compared to the C series.

After 28 days, the unit weights of the K5, K10, and K15 series decreased by 2 %, 4.8 %, and 6.8 %, respectively. The lower specific gravity of K relative to sand contributed to the reduced unit weights observed in the K-replaced mortar series.

UPV measurements are used to detect changes in porosity, crack

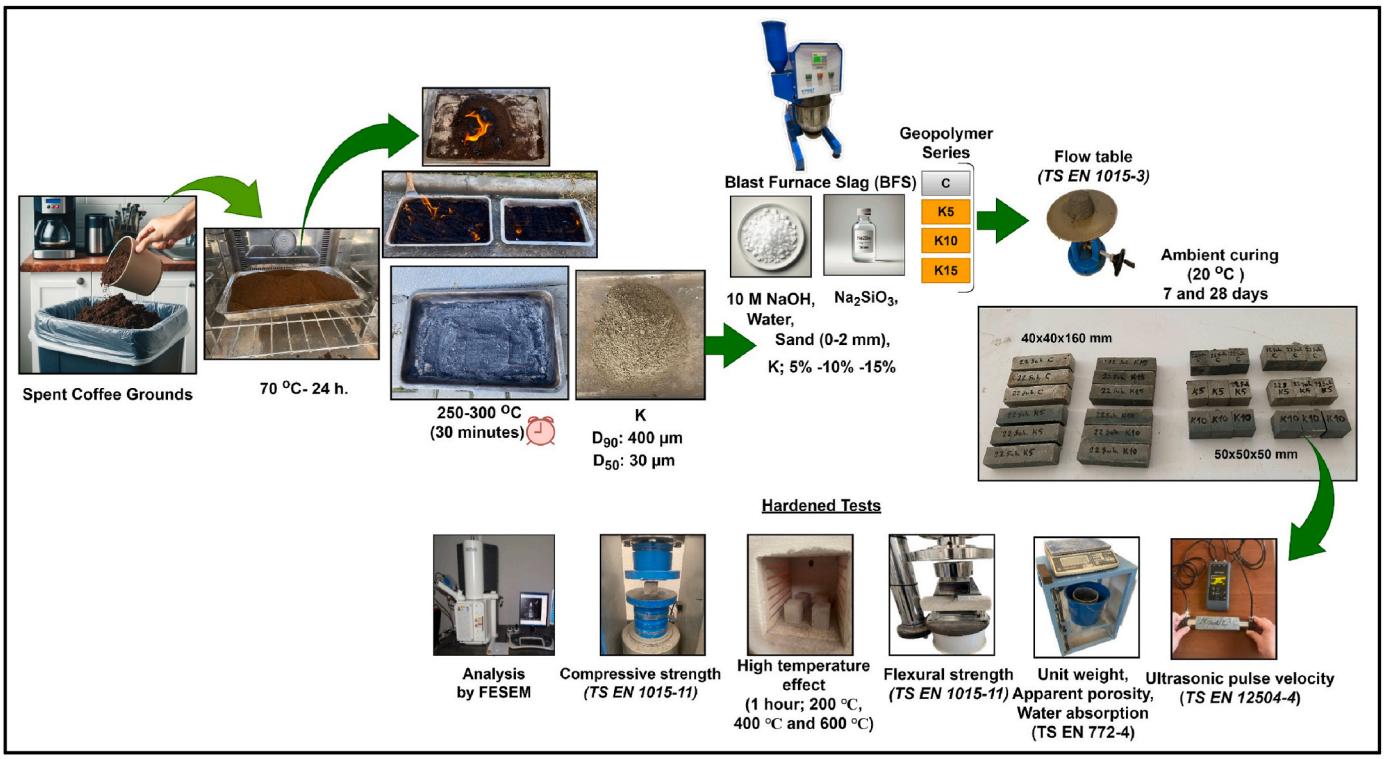

Fig. 6. Flowchart of the mixing and testing procedures.

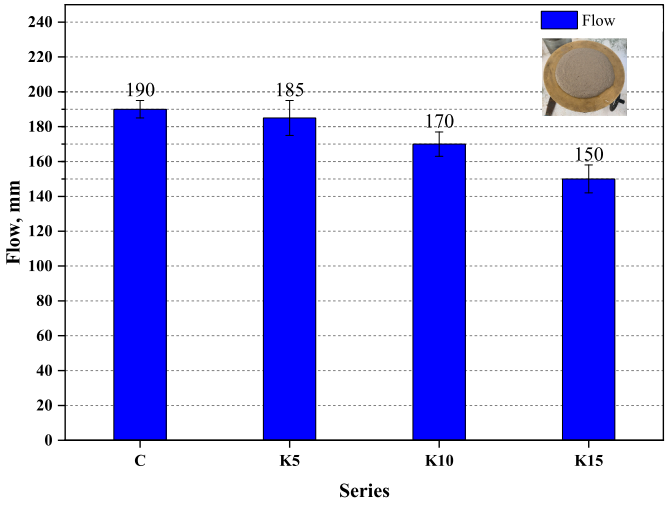

Fig. 7. Flow diameters of geopolymer mortar series.

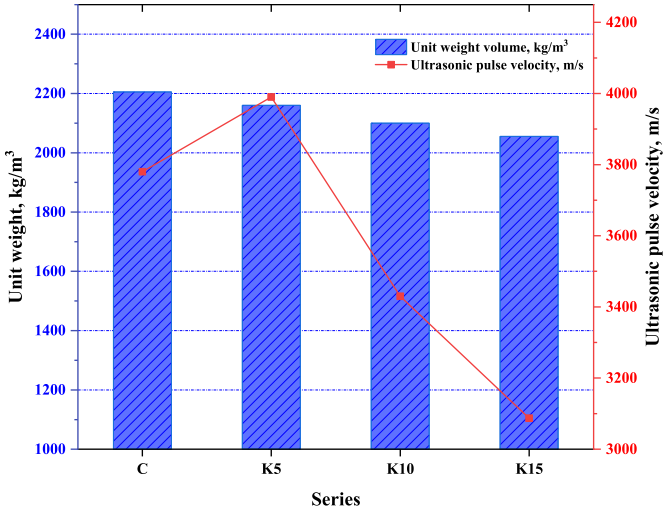

Fig. 8. Unit weight and UPV results of geopolymer mortars.

development, and the progression of polymerization in mortars. The variation in UPV results across the series is presented in Fig. 8. The UPV values ranged from 3087 to 3990 m/s. As shown in Fig. 8, compared to the C series, the UPV values increased by 5.6 % in K5, whereas they decreased by 9.3 % and 18.3 % in K10 and K15, respectively.

As outlined in Section 3.6, the incorporation of 5 % K into the geopolymer mixture reduces apparent porosity by 6.2 % and water absorption by 4 % compared to the control series, confirming an improvement in the matrix structure. This densification is attributed to the greater fineness of K relative to sand, enabling K particles to fill microvoids within the geopolymer matrix, thereby reducing isolated pore spaces and yielding a more compact structure. This reduced porosity at the 5 % replacement level enhances UPV, as ultrasonic waves propagate more efficiently through denser materials.

However, when K replacement exceeds 5 %, the porous and rough nature of K, coupled with its higher water absorption capacity, increases overall void content, as evidenced by significant rises in apparent porosity (+12 % in K10 and + 16.8 % in K15) and water absorption (+28 % in K10 and + 37.3 % in K15), as reported in Section 3.6. This results in a less compact matrix, impeding ultrasonic wave propagation and consequently lowering UPV values. Compressive strength results (Section 3.4) corroborate this trend, with the K5 series exhibiting a 16.3 % increase in compressive strength at 28 days, consistent with improved microstructural integrity and elevated UPV values. Beyond 5 % K replacement, however, compressive strength declines due to increased porosity and reduced geopolymerization efficiency, aligning with the observed UPV reductions. Consequently, UPV values for all series except K5 decrease with higher K replacement rates, suggesting that mortar

samples become more porous relative to the C series as K content increases—a finding supported by internal structure analyses in Section 3.8.

3.3. Flexural strength test results

Flexural strength is a frequently studied parameter in the mechanical behavior of geopolymer mortars, reflecting the material's capacity to resist deformation under load and stress [46]. Fig. 9 displays the 7-day and 28-day flexural strength values of the geopolymer mortar series.

The flexural strengths of the series increased with extended curing times, with the 28-day strengths ranging from 4.9 to 6.3 MPa. As shown in Fig. 9, the 7-day flexural strength of the geopolymer series increased by 13.5 % in K5 compared to the C series, whereas it decreased by 5.8 % and 13.5 % in K10 and K15, respectively. Thus, after the initial 7 days, flexural strength declined with increasing K replacement in all series except for K5. At 28 days, the K5 series exhibited a 6.8 % increase in flexural strength, whereas the K10 and K15 series experienced reductions of 8.5 % and 16.9 %, respectively. The improvement in flexural strength in the K5 series at both 7 and 28 days can be attributed to a lower presence of micro and macro cracks within the mortar matrix and the formation of nearly void-free transition zones between the sand and the geopolymer matrix. It is suggested that incorporating 5 % K improved the transition zone between the geopolymer matrix and the aggregate, thereby enhancing flexural strength. However, the reduction in flexural strength in mortars containing more than 5 % K is attributed to the weak bonding characteristics between the geopolymer matrix and the aggregates. The porous structure of K particles and their high water demand likely contributed to a weakening of bond strength. This phenomenon is also evident in the FESEM images presented in Section 3.8, Fig. 21.

3.4. Compressive strength test results

The compressive strengths of the series after 7 and 28 days of curing are given in Fig. 10. As seen in Fig. 10, the compressive strengths increased with the increase in curing time.

The 7-day compressive strengths of the series ranged from 33.9 to 45.2 MPa, while the 28-day compressive strengths varied between 40.8 and 67.9 MPa. When examining the 7-day compressive strengths of the geopolymer series, it was observed that all series, except for K5, had lower compressive strengths than the C series. After 7 days of curing, the compressive strength of the K5 series showed an 8.9 % increase compared to the C series, whereas K10 and K15 exhibited strength losses

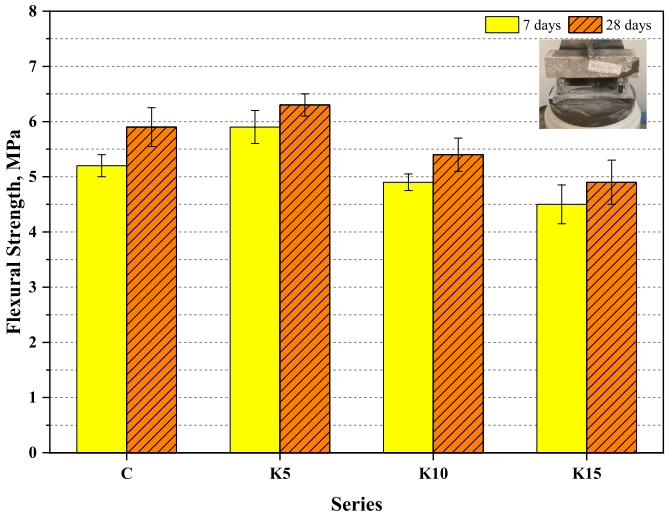

Fig. 9. Flexural strength of geopolymer mortar series after 7 and 28 days.

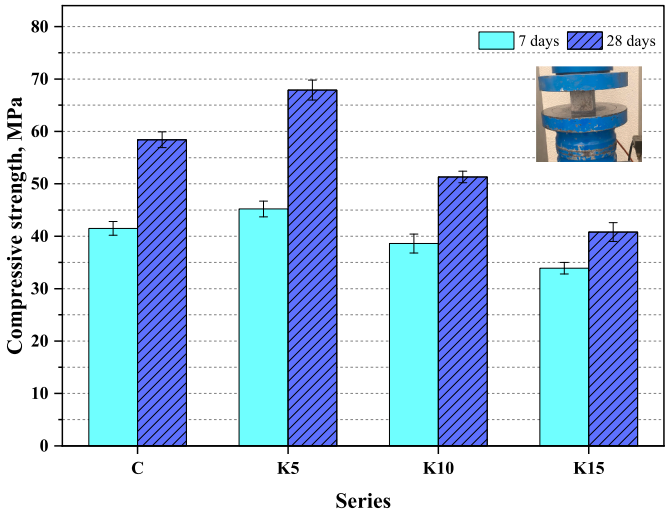

Fig. 10. Compressive strength of geopolymer mortar series at 7 and 28 days.

of 6.9 % and 18.3 %, respectively. Park and Pour-Ghaz [47] found in their study, water in geopolymerization primarily serves as a reaction medium, facilitating the dissolution, transportation, and polymerization of aluminosilicates rather than being permanently integrated into the final geopolymer structure. Water in geopolymerization exists in different states, including evaporable water (which remains in the pore structure and can later evaporate) and chemically bound water, which contributes to the formation and stabilization of the geopolymer matrix. Furthermore, Wang et al. [48] highlighted that the w/b ratio directly affects the setting time, fluidity, and structural integrity of geopolymers. Their study demonstrated that a lower w/b ratio enhances gel densification, while a higher w/b ratio delays setting and weakens the structure due to excessive free water remaining in the matrix. These observations reinforce the idea that an imbalance in available water negatively impacts geopolymerization efficiency and mechanical properties.

Given that K exhibits a higher water absorption capacity than sand, substituting more than 5 % K in the geopolymer blend markedly reduces the availability of free alkaline liquid for reaction with the precursor. This diminished water availability likely impedes the dissolution of aluminosilicates, thereby hindering the formation of a dense geopolymer gel network. Consequently, as similarly noted by Arulrajah et al. [44], elevated K replacement levels adversely impact geopolymerization efficiency, resulting in increased porosity and a corresponding reduction in compressive strength. These findings underscore the need to optimize the water-to-solid ratio and reactive components to balance adequate polymerization with the maintenance of a dense, durable structure. The observed effects correlate with trends in compressive strength, porosity, and UPV, indicating that excessive K replacement elevates void content and diminishes geopolymerization efficiency, thus affecting both microstructural integrity and mechanical performance. Analysis of the 28-day compressive strengths revealed that K5 exhibited a 16.3 % increase, whereas K10 and K15 displayed strength reductions of 12.2 % and 30.1 %, respectively. A comparison of the 7-day and 28-day strength results indicated that the strength losses for K10 and K15 became more pronounced over the 28-day curing period. In a study by Saeli et al. [26], the compressive strength of biomass fly ash-based geopolymer mortars increased by 4.1 % with a 5 % substitution of sand with SCG, yet a 51 % strength loss was observed when the SCG content was raised to 17.5 %. The consistent strength gain in K5 across all curing durations may be attributed to the superior micro-filling capacity of K compared to sand. However, incorporating more than 5 % K into the mixtures led to a strength decline, likely due to K's porous structure and elevated water absorption. As noted in Section 3.6, water absorption and apparent porosity measurements confirmed

that higher K content correlated with increased water absorption rates and void volumes, a finding substantiated by the internal structure analysis in Section 3.8. The relationship between the 7-day and 28-day flexural and compressive strengths of the series is illustrated in Fig. 11, demonstrating a strong linear correlation between these mechanical properties, with R^2 values exceeding 0.9.

3.5. High-temperature behavior

The influence of elevated temperatures on the geopolymer series was examined by assessing mass loss (M), compressive strength (CS), and flexural strength (FS) after exposing the samples to 200 °C, 400 °C, and 600 °C for 1 h. The geopolymer matrix incorporates various forms of water, namely free water, chemically bound water, and hydroxyl groups. These water phases evaporate progressively across distinct temperature ranges, resulting in mass loss and potential crack formation. Free water evaporates between 20 °C and 100 °C, chemically bound water dissociates between 100 °C and 300 °C, and the dehydroxylation of hydroxyl groups occurs above 300 °C, leading to increased porosity and microcracking [49]. This process facilitates moisture release, thereby amplifying mass loss at elevated temperatures. Furthermore, the resulting microcracks enhance permeability, allowing trapped water to evaporate more efficiently beyond 400 °C, which further accelerates mass loss [50]. With increasing temperature, mass loss in all geopolymer mortar series exhibited a corresponding increase (Fig. 12). This effect is primarily attributed to the evaporation of free water from the mortar matrix as the temperature rises. The progressive removal of water at elevated temperatures leads to the gradual drying of the material. Experimental results demonstrated that within the temperature range of 20–400 °C, the evaporation of free water caused significant mass loss. However, beyond 400 °C, the rate of mass loss declined and nearly stabilized at 600 °C. This phenomenon is attributed to the significant removal of water from the samples at 400 °C, resulting in a reduced rate of further evaporation at higher temperatures. Additionally, exposure to elevated temperatures induces the formation of microcracks due to incompatibilities arising from differences in the thermal expansion coefficients of the aggregate and the mortar matrix. These microcracks, coupled with increased porosity, facilitate moisture loss by creating pathways for water evaporation, particularly at higher temperatures. Moreover, the thermal mismatch between the aggregate and the paste generates internal stresses, exacerbating crack propagation and ultimately amplifying the overall mass loss in geopolymer mortars [51]. The results revealed that the greatest mass loss occurred in the K15 series, while the smallest mass loss was observed in the C series. This phenomenon can be attributed to the higher initial porosity and

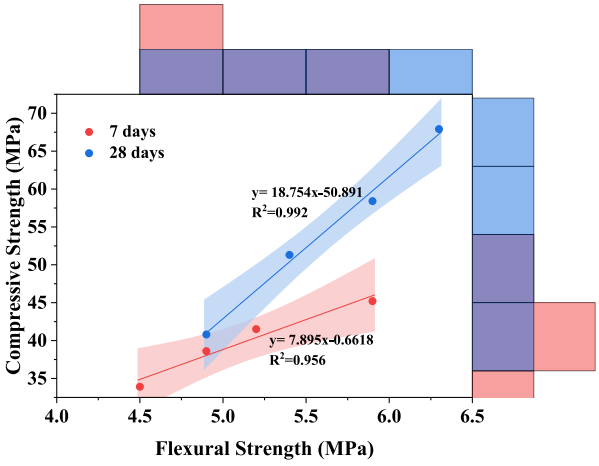

Fig. 11. Relationship between 7-day and 28-day flexural and compressive strengths across the series.

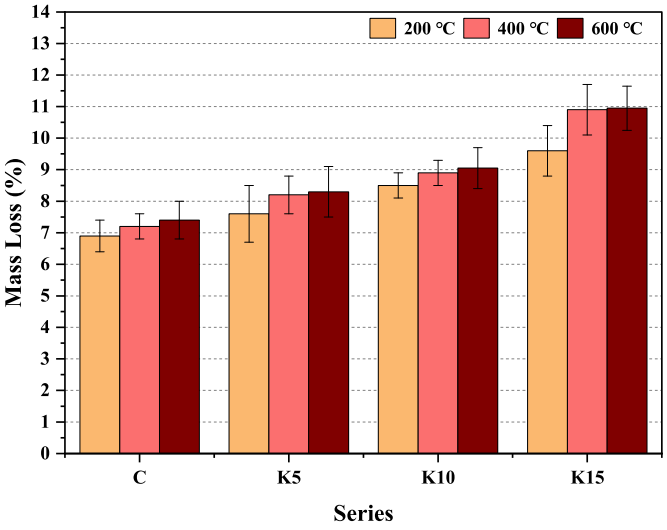

Fig. 12. Mass loss of the series after exposure to high temperatures (%).

water absorption capacity of K. Following exposure to elevated temperatures, the mortar series were physically examined for cracking and spalling damage. As reported in the literature [52], the recrystallization of geopolymers at high temperatures is considered one of the key factors enabling geopolymers to retain their structural integrity after heat exposure. Fig. 13 illustrates the physical appearance of the series before and after exposure to various temperatures, showing a shift from dark gray to white as temperature increased, with samples retaining their shape up to 600 °C.

This color change is primarily attributed to two factors: (i) the oxidation and decomposition of organic residues in the K series, and (ii) phase transformations within the geopolymer matrix. The initial dark gray color of the K series likely stems from residual organic compounds, which, when heated, oxidize and decompose, reducing carbonaceous matter and lightning the surface [53]. Additionally, in BFS-based

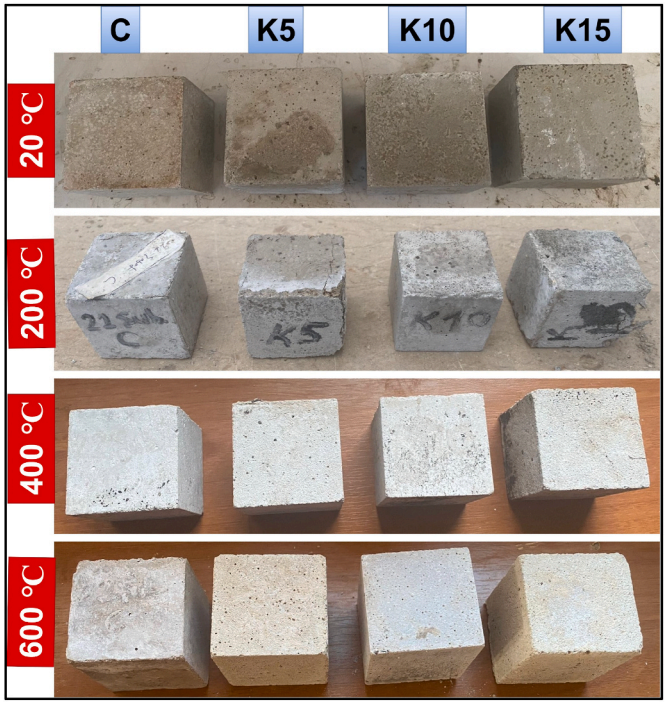

Fig. 13. Appearance of the specimens before and after exposure to high temperatures.

geopolymer mortars, structural changes above 400 °C, including the formation of crystalline phases and sintering of amorphous phases, further contribute to whitening. Similar transitions have been observed in BFS- and fly ash-based geopolymers after thermal exposure [54,55].

Fig. 14 illustrates the temperature-dependent changes in the compressive strength of the geopolymer mortar series. The compressive strength of the geopolymer mortar samples decreased markedly with increasing temperature. BFS-based geopolymers exposed to elevated temperatures exhibit a progressive reduction in compressive strength, attributed to alterations in the mortar matrix and the mortar-aggregate transition zone. The incompatibility between the contracting mortar and the expanding quartz aggregates induces cracking and increases porosity. However, above 600 °C, the rate of strength reduction slows considerably [56]. At 200 °C, the compressive strength of the C, K5, K10, and K15 series decreased by approximately 7.2 %, 6.6 %, 6.0 %, and 13.7 %, respectively. This reduction in compressive strength became more pronounced with further increases in temperature.

The compressive strengths of the C, K5, K10, and K15 series decreased by 28.4 % and 45.7 %, 28.3 % and 42.3 %, 26.5 % and 39.2 %, and 31.9 % and 58.8 %, respectively, after exposure to 400 °C and 600 °C. These results suggest that, among the geopolymer mortar series, K5 and K10 exhibited the highest resistance to compressive strength loss at elevated temperatures. In contrast, the K15 series experienced the most significant reduction in strength.

Fig. 15 illustrates the temperature-dependent variations in the flexural strength of the geopolymer mortar series. At 200 °C, the flexural strength of the C, K5, K10, and K15 samples decreased by approximately 9.5 %, 5.6 %, 8.5 %, and 15.7 %, respectively. This reduction in flexural strength became more pronounced with increasing temperatures. At 400 °C and 600 °C, the flexural strength reductions for the C, K5, K10, and K15 series were recorded as 31.0 % and 47.5 %, 29.4 % and 48.6 %, 30.9 % and 47.2 %, and 32.9 % and 62.7 %, respectively.

As reported in the literature [50,57,58], the evaporation of water and matrix degradation at elevated temperatures result in the expansion of the pore structure and the formation of microcracks, thereby reducing the strength of geopolymers. Increasing temperatures further weaken the material by loosening the microstructure. Nevertheless, after exposure to high temperatures, the specimens retain their original dimensions, with no evidence of spalling, fragmentation, or macro-level cracking observed along the outer surfaces (Fig. 13). This stability can be attributed to the inherent physical properties of the K series, particularly its high porosity and void content within the microstructure. Moreover, the increased porosity of the K series likely provided pathways within the material, facilitating the release of water vapor at 400 °C and 600 °C. This may explain why the strength loss in the K5 and K10 series after exposure to elevated temperatures was lower than that observed in the other series. The relationship between the flexural and compressive strengths of the series across various temperatures is presented in Fig. 16. Strong linear correlations, with R^2 values exceeding 0.9, were identified between these strengths. The highest correlations were observed at 20 °C and 200 °C, whereas the R^2 values progressively decreased with increasing temperature.

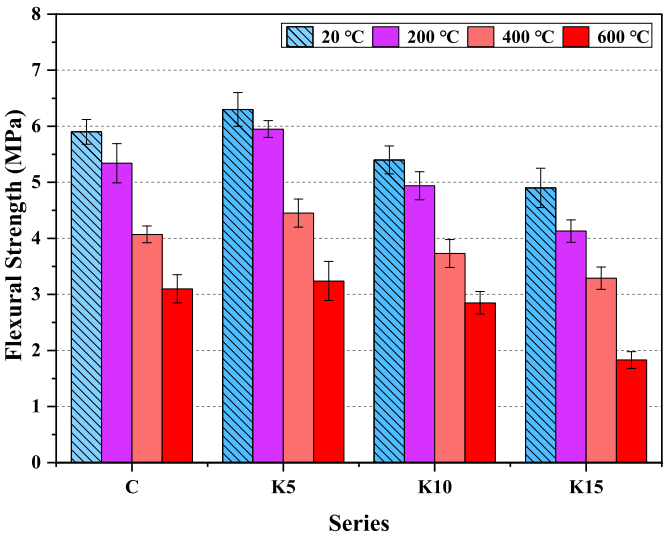

Fig. 15. Residual flexural strengths of the series after exposure to various temperatures.

3.6. Apparent porosity and water absorption test results

The variation in apparent porosity and water absorption values of the mortar series after 28 days of curing is illustrated in Fig. 17. The apparent porosity values for the series ranged between 7.8 % and 9.7 %, whereas the water absorption values varied from 3.6 % to 5.2 %.

The presence of pores and cracks in concrete increases water absorption, which adversely impacts the durability and long-term performance of the concrete [59]. Generally, the results of the apparent porosity and water absorption tests indicate a directly proportional relationship with the K content in the series (with the exception of K5);

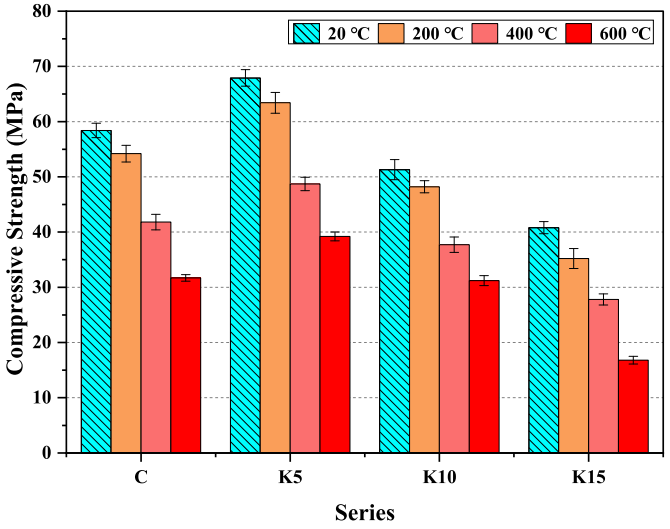

Fig. 14. Residual compressive strengths of the series after exposure to various temperatures.

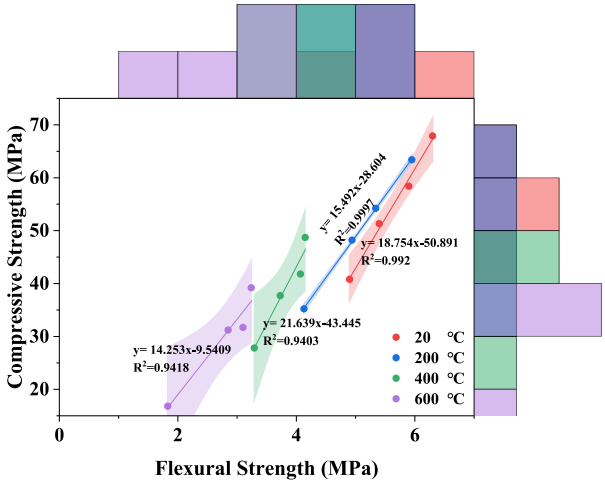

Fig. 16. Relationships between the flexural and compressive strengths of the series at various temperatures.

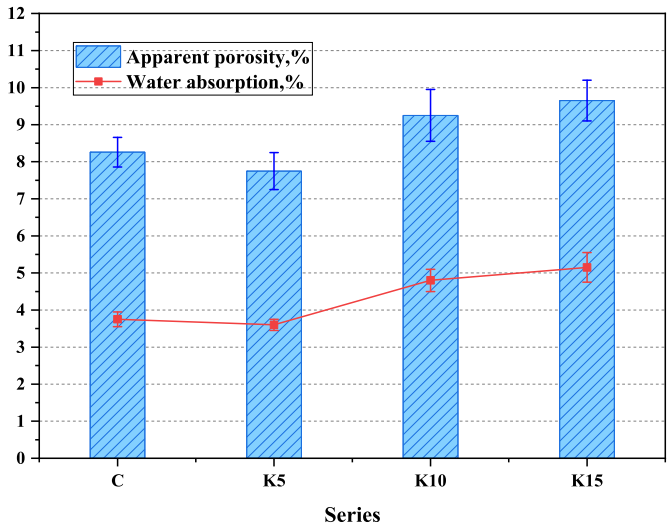

Fig. 17. Apparent porosity and water absorption percentages of the series at 28 days.

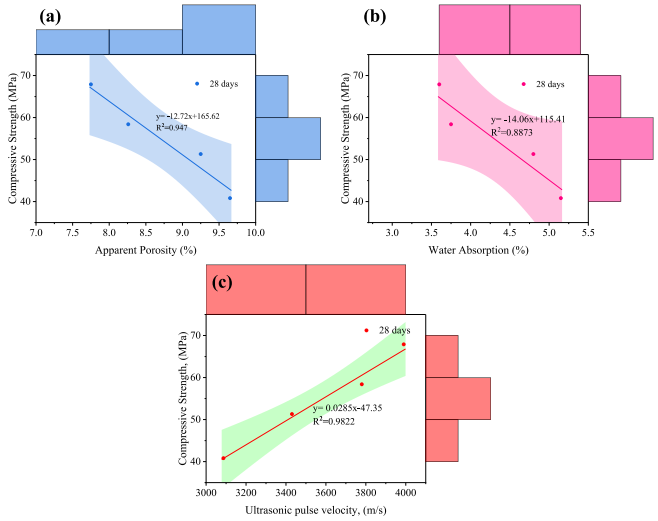

Fig. 18. Relationships between the compressive strength and the physical properties of the series: (a) apparent porosity, (b) water absorption, and (c) ultrasonic pulse velocity (UPV).

that is, as the K content increases, both the apparent porosity and water absorption rates rise accordingly. Fig. 15 illustrates that the apparent porosity values of the series, compared to the C series, decreased by 6.2 % in K5, while increasing by 12 % and 16.8 % in K10 and K15, respectively. Similarly, the water absorption rates decreased by 4 % in K5, whereas they increased by 28 % and 37.3 % in K10 and K15, respectively. Based on these results, it can be inferred that substituting 5 % K in the mortar mix enhances both the apparent porosity and water absorption properties. This improvement with a 5 % K replacement can be attributed to its capacity to fill the pores within the mortar matrix, thereby facilitating the formation of new products, promoting a denser molecular structure, and reducing the porosity of the geopolymer mortar over time. Furthermore, the greater fineness of K compared to sand (Fig. 3) may have contributed to the filling of micro-pores in the K5 series. However, the incorporation of K beyond 5 % in the geopolymer mixtures progressively increases the water absorption capacity. This effect is likely due to the rough and porous nature of K [44], coupled with the formation of pores in the specimens, as evidenced by the microstructure analysis.

Fig. 18 presents the relationships and corresponding equations between the 28-day apparent porosity (a), water absorption percentages (b), and UPV values (c) with the compressive strength of the series. As depicted in Fig. 18, an increase in apparent porosity and water absorption percentages is associated with a decrease in compressive strength, reflecting a strong negative correlation (R^2 values of 0.947 and 0.8873, respectively). Furthermore, it was observed that an increase in the UPV values of the series corresponds to an increase in compressive strength, demonstrating a robust linear relationship between these parameters ($R^2 = 0.9822$).

3.7. Statistical evaluations

This section elucidates the relationships between the flow table spread values (F) of the produced mortar series, the compressive strength (CS), flexural strength (FS), and mass loss (M) results following exposure to temperatures of 200, 400, and 600 °C for 28-day samples, and the design parameters: K content (%) and applied temperature (T; °C). To this end, multiple linear regression analyses were performed, complemented by the generation of analysis of variance (ANOVA) and Pearson correlation matrices. In these analyses, F, CS, FS, and M were designated as dependent variables, while K and T were treated as independent variables. All analyses were conducted with a 95 % confidence interval, and the extent of the influence of the independent variables on the dependent variables was quantified.

The predictive capability of the regression models presented in this study is valid within the specific conditions (K replacement level, applied temperature values, and curing duration) and parameter ranges employed during model development. These constraints should be considered when applying the models to conditions outside the scope of those investigated.

The objective of the multiple regression model is to maximize the explanation of the dependent variable using the fewest possible explanatory variables. The dependent variable is expressed as a function of independent variables with specific coefficients. Unlike simple regression, multiple regression incorporates more than one independent variable. Most multiple regression equations conform to the form presented in Equation (3.1) [60,61].

$$y = a_1x_1 + a_2x_2 + a_3x_3 + \ldots \ldots + a_nx_n + C \tag{3.1}$$

In this study, the analysis of variance (ANOVA) results for compressive strength (CS), flexural strength (FS), and mass loss (M), obtained following exposure to high temperatures (T) across all series, are presented in Table 3. The F-statistic, mean square, p-value, and degrees of freedom (df) are utilized to interpret the relationships between the variables in the ANOVA. A p-value less than 0.05 indicates that the coefficients in the model are statistically significant [62].

The effectiveness of multiple regression analysis (MRA) relies on the assumption of linearity between the independent variables and the dependent variable, as well as the independence of observations. High levels of multicollinearity or strong correlations among the independent variables can complicate the analysis. To evaluate the presence of autocorrelation among the variables, the Durbin-Watson test was employed, as outlined in Equation (3.2). The test value is expected to fall between 1.5 and 2.5 [63]. In this study, the Durbin-Watson test yielded values ranging from 1.5 to 2.2 (Table 3), confirming that the assumption of no autocorrelation was satisfied. Consequently, the reliability and validity of the MRA were substantiated.

$$\text{Durbin} - \text{Watson value} = \frac{\sum_{n=2}^{N} x_n - (x_n - 1)^2}{\sum_{n=1}^{N} (x_n)^2} \tag{3.2}$$

Where n represents the total number of observations, and x_n denotes the nth residual of the regression model.

Table 3
Analysis of variance for F, CS, FS, and M in the geopolymer series.

Model		Sum of squares	df	Mean square	F	p-value	Durbin Watson value
Flow, (F)	Regression	911.25	1	911.25	31.696	0.03	2.03
Predictors: (Constant), K	Residual	57.5	2	28.75	–		
	Total	968.75	3	–	–		
Compressive	Regression	2250.309	2	1125.154	25.731	<0.001	2.207
Strength, (CS)	Residual	568.461	13	43.728	–	–	
Predictors: (Constant), K,T	Total	2818.769	15	–	–	–	
Flexural Strength, (FS)	Regression	22.526	2	11.263	72.839	<0.001	2.017
Predictors: (Constant), K,T	Residual	2.010	13	0.155	–	–	
	Total	24.536	15	–	–	–	
Mass loss, (M)	Regression	9.989	2	4.995	143.346	<0.001	1.503
Predictors: (Constant), K,T	Residual	0.314	9	0.035	–	–	
	Total	10.303	11	–	–	–	

Based on the results of the statistical evaluation, it was determined that there is negligible correlation between the independent variables K and T. The regression analysis indicated that 79.8 % of the variance in compressive strength (CS) values ($R^2 = 0.798$), 91.8 % of the variance in flexural strength (FS) values ($R^2 = 0.918$), and 97 % of the variance in mass loss (M) values ($R^2 = 0.97$) were significantly influenced by the independent variables K and T. In other words, 79.8 % of the variation in CS, 91.8 % of the variation in FS, and 97 % of the variation in M can be attributed to the combined effects of K and T. The p-values for both independent variables (K and T) were less than 0.05, confirming that these variables are statistically significant in predicting the CS, FS, and M values of the mortar series. Furthermore, it was observed that K and T exhibit a negative relationship with CS and FS, while demonstrating a positive relationship with M.

The model equations derived from the statistical analysis are presented below in Equations (3.3)–(3.6).

$$F = 194 + (-2.7)*K \tag{3.3}$$

$$CS = 66.214 + (-0.044)*T + (-1.236)*K \tag{3.4}$$

$$FS = 6.479 + (-0.005)*T + (-0.079)*K \tag{3.5}$$

$$M = 6.406 + (0.002)*T + (0.156)*K \tag{3.6}$$

F: Flow table diameter (mm); CS: Compressive strength (MPa); FS: Flexural strength (MPa); M: Mass loss (%); K: K replacement level (%); T: Temperature (°C).

The models presented in Equations (3.3)–(3.6) were employed to predict the F, CS, FS, and M values of the geopolymer mortar series produced in this study. The relationships between the experimental results obtained from the series and the predicted values are illustrated in Fig. 19. The predicted models and experimental data exhibit a 'very strong' linear relationship ($R^2 > 0.9$) for F, FS, and M, while a 'good' linear relationship ($R^2 = 0.7983$) is observed for CS.

The results of the statistical evaluation revealed that K content (%) and applied temperature (T) exert a statistically significant influence on the compressive strength (CS), flexural strength (FS), and mass loss (M) of the geopolymer mortars. According to the sensitivity analysis (Table 4), the contributions of K and T to CS were 45 % and 53.7 %, respectively, while their contributions to FS were 18.6 % and 80.4 %, and to M were 89.6 % and 9.4 %, respectively. The analysis indicated that T had the most substantial impact on the CS and FS outcomes of the geopolymer mortars, whereas K content exerted the predominant effect on the M outcomes.

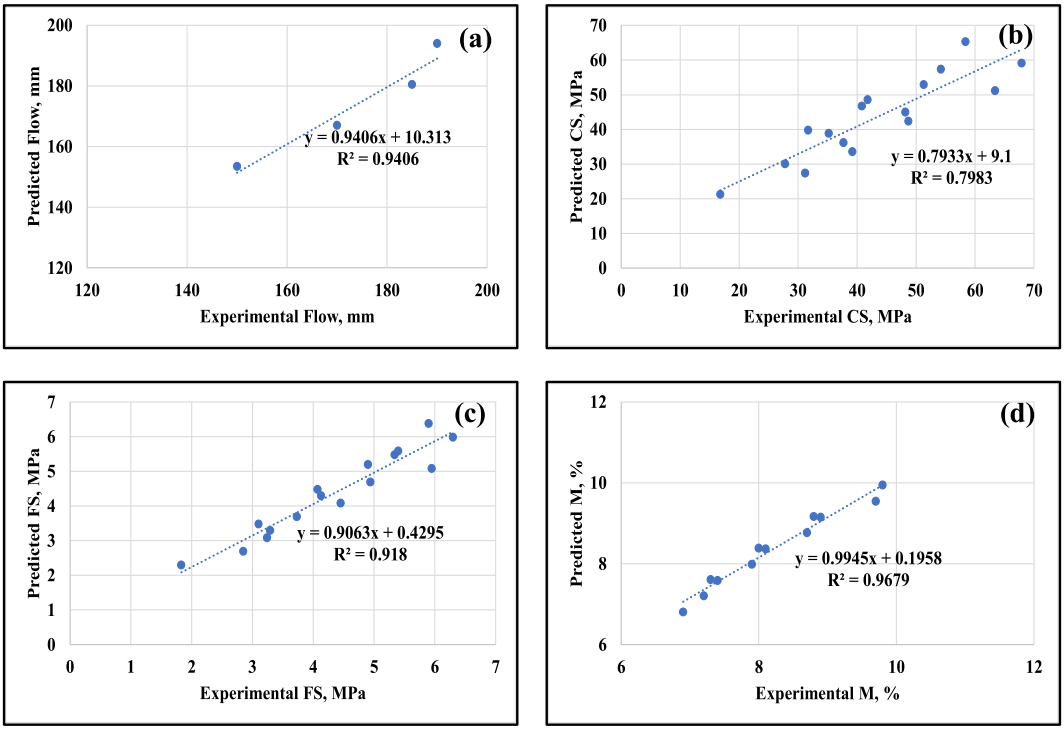

Fig. 19. Relationships between predicted and experimental results for the geopolymer mortar series: (a) Flow, (b) CS, (c) FS, (d) M.

Table 4
Statistical analysis of strength test results.

Dependent variable	Independent variable	Statistical parameters				
		Sequential sum of squares	Mean square	F	p-value	Contribution
Compressive Strength, (CS)	K replacement level (%)	1267.912	422,637	105.819	0.000	45 %
	T (temperature °C)	1514.912	504,971	126.434	0.000	53.7 %
	Error	35.946	3994	–	–	1.3 %
	Total	2818.769	–	–	–	–
Flexural Strength, (FS)	K replacement level (%)	4.564	1.521	57.058	0.000	18.6 %
	T (temperature °C)	19.732	6.577	246.674	0.000	80.4 %
	Error	0.240	0.027		–	0.1 %
	Total	24.536			–	–
Mass loss, (M)	K replacement level (%)	9.237	3.079	193.383	0.000	89.6 %
	T (temperature °C)	0.970	0.485	30.463	0.001	9.4 %
	Error	0.096	0.016	–	–	0.9 %
	Total	10.303	–	–	–	–

Correlation matrices illustrate the relationships among parameters. A correlation coefficient exceeding 0.8 between two properties suggests a strong linear relationship [59]. The Pearson correlation matrix, developed to demonstrate the extent of the relationships between the design parameters (K and T) and the experimental results (CS, FS, and M), is presented in Fig. 20.

Pearson correlation coefficients range from +1 to −1. Accordingly, a value of '+1′ denotes a perfect positive correlation, '-1′ signifies a perfect negative correlation, and '0′ indicates no correlation. In assessing correlation strength, coefficients between 0.4 and 0.6 are classified as 'moderate,' those between 0.6 and 0.8 as 'good,' and those between 0.8 and 1.0 as 'strong.' Positive correlations are represented in red, whereas negative correlations are depicted in blue.

According to Fig. 20, a moderate negative correlation exists between CS and K (Pearson −0.52), while a strong negative correlation is observed between CS and T (−0.73). This indicates that increasing K moderately reduces CS, whereas increasing T markedly lowers CS. No correlation exists between K and T (0), suggesting their independence. Similarly, FS shows a weak negative correlation with K (−0.36) and a very strong negative correlation with T (−0.89), implying that increasing K slightly decreases FS, while increasing T substantially reduces FS. Conversely, a very strong positive correlation is found between K and M (0.94), and a weak positive correlation between T and M (0.28), indicating that increasing K significantly increases M, whereas increasing T results in a marginal increase in M.

3.8. Microstructure analysis

Microstructure analysis is a critical method for elucidating the effects of K on BFS-based geopolymer mortar. The geopolymer mortar series were air-cured at ambient temperature from the time of production until the 28th day. Following curing, the internal structure of samples obtained from C, K5, K10, and K15 was analyzed using a ZEISS Supra 40 V P field emission scanning electron microscope (FESEM), as shown in Figs 21 and 22.

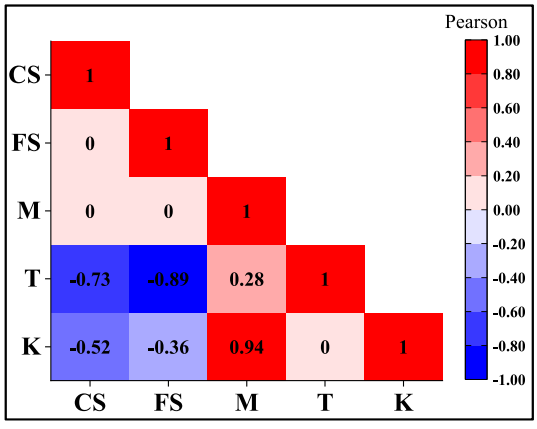

Fig. 20. Pearson correlation matrices illustrating relationships between design parameters and test results of the geopolymer mortar series.

In the geopolymer mortar series, the formation of dense C–A–S–H (calcium aluminosilicate hydrate) and N–A–S–H (sodium aluminosilicate hydrate) binding phases was observed. Studies in the literature [27, 45] have demonstrated that when BFS, a calcium-rich precursor, is used, the primary reaction products of the alkali-activated binder are C–S–H and C–A–S–H gels. Additionally, N–A–S–H-type gels are likely to coexist as minor secondary products alongside C–A–S–H-type gels across most of the compositional range of alkali-activated BFS [64]. The elevated silica (SiO_2) and alumina (Al_2O_3) content in BFS provides a suitable matrix for geopolymerization, while its high calcium oxide (CaO) content promotes the formation of hydration products. The mortar matrices of the C and K5 series exhibited a dense and homogeneous microstructure with a predominantly smooth surface morphology. In the K5 series, the absence of a distinct boundary between the aggregate and the geopolymer matrix suggests a strong interfacial bond and indicates the role of K in micro-pore filling (Fig.s 21(b) and 22(a)). While the fineness of K is hypothesized to enhance micro-pore filling and contribute to the observed densification in the K5 series, further studies incorporating particle size analysis and porosity measurements are recommended to substantiate this relationship. Furthermore, previous studies have demonstrated that the incorporation of fine materials can enhance matrix densification by reducing interfacial porosity and refining the pore structure [65–69]. Our findings align with these studies, supporting the hypothesis that the fine particles of K contribute to micro-pore filling during the geopolymerization process.

The microcracks and visible voids observed in the internal structure of the K10 and K15 series (Fig.s 21(c), 21(d), and 22(b)) are attributed to rapid early strength development and the evaporation of unreacted free water. As observed in Fig. 21(c), some BFS particles (visible as bright white regions) may not have fully reacted during the geopolymerization process, resulting in the presence of anhydrous phases within the matrix. Additionally, fresh mortar tests revealed that the high water absorption capacity of K caused water to be absorbed by its particles in the fresh state, which evaporated from the matrix during curing, creating voids in certain areas. Consistently, Eryılmaz and Polat [70] reported that incorporating recycled geopolymer aggregates with high water absorption capacity into geopolymer mixtures resulted in void formation within the matrix, attributing this to water absorbed in the fresh state evaporating during curing and leaving voids in certain regions. This resulted in diminished mechanical properties in the geopolymer mortar series with high K content, such as K10 and K15. FESEM images of the K15 series further reveal unfilled pores within the matrix, suggesting that the integrity of the mortar matrix deteriorated with increasing K content, thereby contributing to structural weaknesses. The elevated

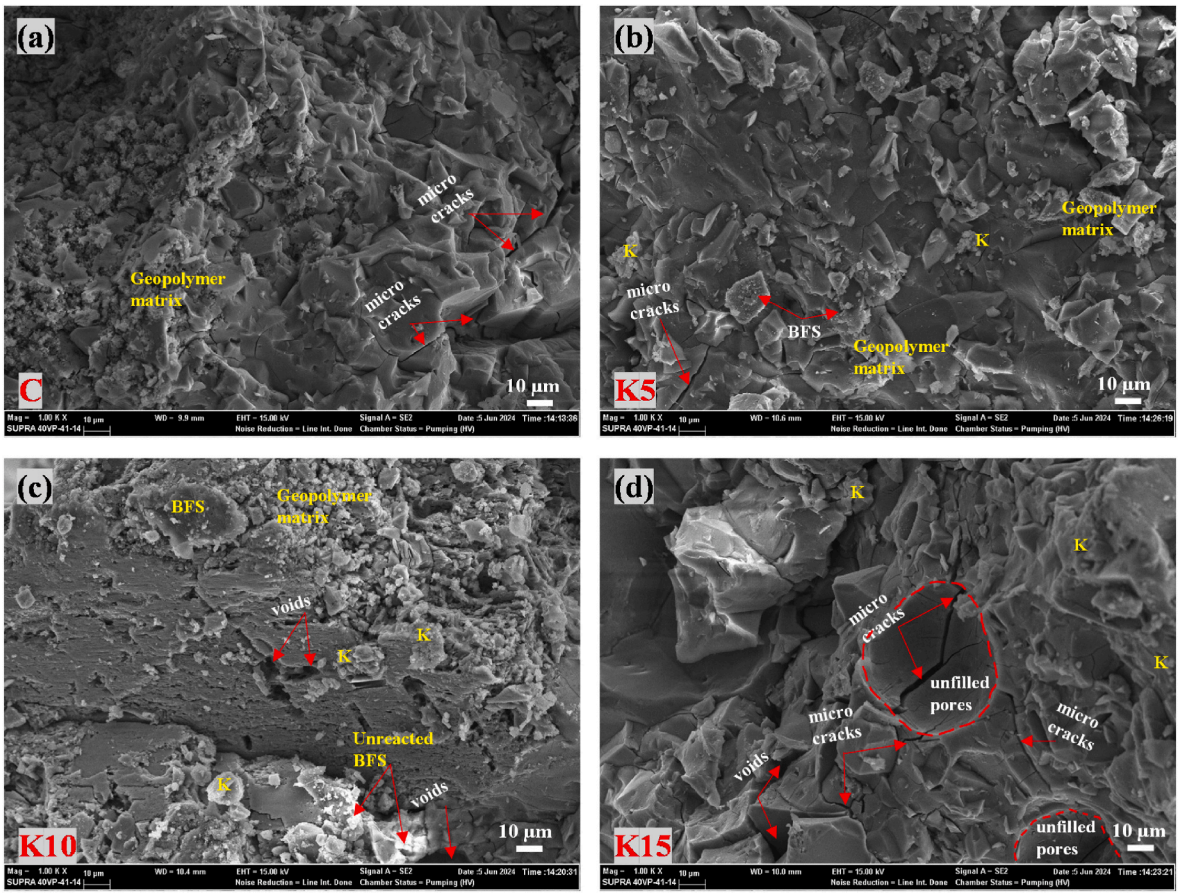

Fig. 21. FESEM images of the series (× 1000 magnification): (a) C, (b) K5, (c) K10, (d) K15.

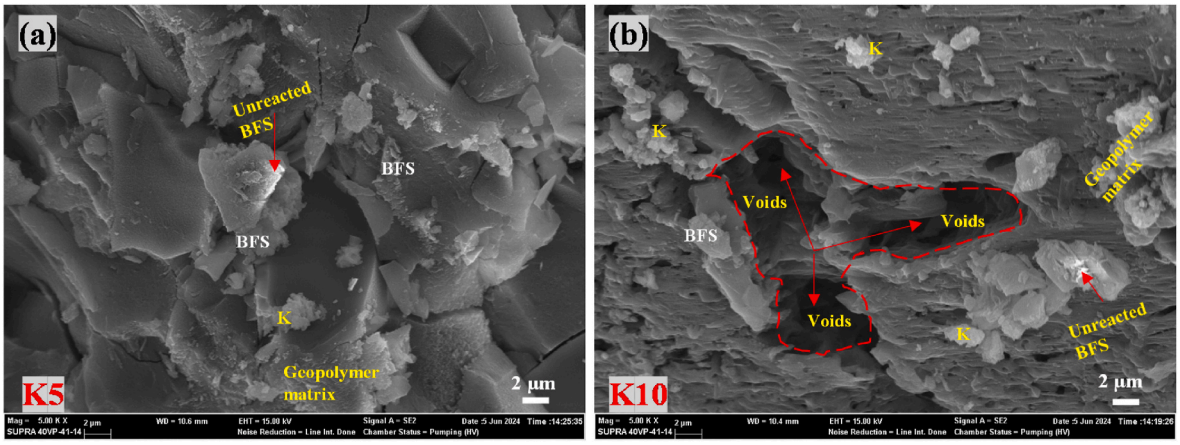

Fig. 22. FESEM images (×5000 magnification) of series: (a) K5, (b) K10.

K_2O content in K may react with NaOH and Na_2SiO_3 solutions, potentially leading to an excess of alkali activation products. This excess could induce crystallization and microcracking under highly alkaline conditions. Mechanical test results confirm that these factors adversely affected the mechanical properties of the mortar.

The presence of pores and microcracks offers valuable insights into the durability and strength of the mortar. A comparison of the internal structures of the C and K5 series revealed that the K5 series, containing 5 % K, exhibited microcracks that were less dense and narrower than those in the C series. This reduced microcrack density likely helps preserve material integrity, thereby enhancing mechanical strength, particularly compressive strength. As indicated in Table 1, K contains CaO (12.35 %) and MgO (7.52 %), which may contribute to the strength of the geopolymerization process. While CaO may support matrix densification through the formation of gels such as calcium silicate hydrate (C–S–H) [71], MgO could also play a role in enhancing mechanical properties. For instance, Hu et al. [72] suggest that MgO may facilitate the formation of magnesium silicate hydrate (M–S–H) gels, potentially increasing microstructural compactness. Similarly, Bernal et al. [73] indicate that MgO might promote the development of hydrotalcite-like phases, which could coexist with other gels to improve microstructural stability and contribute to strength over time. In summary, MgO may enhance

strength by supporting the formation of M–S–H gels and hydrotalcite-like phases, which could reinforce the matrix's integrity and durability. Furthermore, in the K5 series (Fig. 22(a)), a strong bond between the aggregate and the matrix was observed. This robust interfacial bonding is believed to enhance the flexural strength of the K5 series by facilitating more effective load transfer.

4. Conclusions

This study investigates the effects of ash (K) derived from the incineration of SCG on the workability, physical properties, mechanical performance, microstructural characteristics, and high-temperature behavior of ambient-cured BFS-based geopolymer mortars. The findings, based on experimental and statistical analyses, are presented below. In this context.

- The replacement of sand with K in geopolymer mortars increased the water demand of the mixture due to K's finer particle size and porous structure compared to sand. Consequently, incorporating K at levels up to 15 % reduced the workability of the series at all levels, resulting in a workability reduction of up to 21 %.
- The K5 series exhibited compressive strength increases of 8.9 % and 16.3 % after 7 and 28 days of curing, respectively, compared to the C series, whereas the compressive strengths of the K10 and K15 series decreased across all curing periods. Comparable trends were observed in flexural strength.
- Under high-temperature conditions, the K15 series exhibited the greatest mass loss, whereas the C series showed the least. As the temperature increased to 400 °C, substantial mass losses were observed across all series. However, at 600 °C, mass loss in all series nearly stabilized, with samples retaining their physical integrity. Additionally, the K5 and K10 series demonstrated the highest resistance to elevated temperatures in terms of strength retention, whereas the K15 series experienced the most significant strength loss.
- The apparent porosity and water absorption by weight ranged from 7.8 % to 9.7 % and from 3.6 % to 5.2 %, respectively. In all series except for K5, both apparent porosity and water absorption increased with increasing K content.
- According to the developed multiple regression models, T (°C) exerted the strongest influence on the CS and FS of the mortars, whereas K (%) had a greater impact on M (%). This finding is expected to significantly aid researchers in optimizing mix designs, thereby reducing costs and experimental time.
- Microstructure analyses of the mortar series revealed that the K5 series exhibited strong bonding between the geopolymer matrix and the aggregate, low crack formation, and a more homogeneous structure. In contrast, the K10 and K15 series displayed a higher number of microcracks and pores compared to the other series, which was assessed to have a negative impact on their mechanical strengths.
- In conclusion, further studies utilizing additional aluminosilicate sources, such as metakaolin or fly ash, or alternative alkaline activators, such as potassium hydroxide or potassium silicate, are recommended. These studies are intended to improve the mechanical strength, durability, and thermal resistance of geopolymer mortars in which K replaces aggregate, thereby contributing to a more efficient mix design.

Declaration of competing interest

The authors declare that they have no known competing financial interests or personal relationships that could have appeared to influence the work reported in this paper.

References

[1] A.F. Şenol, C. Karakurt, Öğütülmüş pişmiş kil ve mermer atıklarının çimentolu harçlarda dayanım gelişimine etkisi, Iğdır Üniversitesi Fen Bilimleri Enstitüsü Dergisi 13 (4) (Dec. 2023) 2692–2705, https://doi.org/10.21597/jist.1311857.

[2] F. Faleschini, C. Jiménez, M. Barra, D. Aponte, E. Vázquez, C. Pellegrino, Rheology of fresh concretes with recycled aggregates, Constr. Build. Mater. 73 (2014), https://doi.org/10.1016/j.conbuildmat.2014.09.068.

[3] F. Li, L. Liu, ZhemingYang, S. Li, Influence of modified multi-walled carbon nanotubes on the mechanical behavior and toughening mechanism of an environmentally friendly granulated blast furnace slag-based geopolymer matrix, Ceram. Int. 47 (1) (2021), https://doi.org/10.1016/j.ceramint.2020.08.203.

[4] V.K. Singh, G. Srivastava, Development of a sustainable geopolymer using blast furnace slag and lithium hydroxide, Sustainable Materials and Technologies 40 (Jul. 2024) e00934, https://doi.org/10.1016/J.SUSMAT.2024.E00934.

[5] A. Raif Boğa, A. Ferdi Şenol, The effect of waste marble and basalt aggregates on the fresh and hardened properties of high strength self-compacting concrete, Constr. Build. Mater. 363 (2023), https://doi.org/10.1016/j.conbuildmat.2022.129715.

[6] C. Suksiripattanapong, T.A. Kua, A. Arulrajah, F. Maghool, S. Horpibulsuk, Strength and microstructure properties of spent coffee grounds stabilized with rice husk ash and slag geopolymers, Constr. Build. Mater. 146 (2017), https://doi.org/10.1016/j.conbuildmat.2017.04.103.

[7] T.A. Kua, A. Arulrajah, S. Horpibulsuk, Y.J. Du, S.L. Shen, Strength assessment of spent coffee grounds-geopolymer cement utilizing slag and fly ash precursors, Constr. Build. Mater. 115 (2016), https://doi.org/10.1016/j.conbuildmat.2016.04.021.

[8] B.A. Tayeh, B. Bayrak, A.M. Zeyad, G. Kaplan, A. Öz, A.C. Aydın, Effect of hybrid fibers and high temperatures on the properties of geopolymer composites based on slag, metakaolin, and natural zeolite, Constr. Build. Mater. 451 (Nov. 2024) 138898, https://doi.org/10.1016/J.CONBUILDMAT.2024.138898.

[9] A.M. Zeyad, O.Y. Bayraktar, B.A. Tayeh, A. Öz, İ.G.M. Özkan, G. Kaplan, Impact of rice husk ash on physico-mechanical, durability and microstructural features of rubberized lightweight geopolymer composite, Constr. Build. Mater. 427 (May 2024) 136265, https://doi.org/10.1016/J.CONBUILDMAT.2024.136265.

[10] N. Yong-Sing, et al., Thin fly ash/ladle furnace slag geopolymer: effect of elevated temperature exposure on flexural properties and morphological characteristics, Ceram. Int. 48 (12) (2022), https://doi.org/10.1016/j.ceramint.2022.02.201.

[11] B. Bayrak, S.A. Mostafa, A. Öz, B.A. Tayeh, G. Kaplan, A.C. Aydın, The effect of clinker aggregate on acid resistance in prepacked geopolymers containing metakaolin and quartz powder in the presence of ground blast furnace slag, J. Build. Eng. 69 (Jun. 2023) 106290, https://doi.org/10.1016/J.JOBE.2023.106290.

[12] S.J. Chithambaram, S. Kumar, M.M. Prasad, Thermo-mechanical characteristics of geopolymer mortar, Constr. Build. Mater. 213 (2019), https://doi.org/10.1016/j.conbuildmat.2019.04.051.

[13] X. Zhang, et al., Thermal behavior and mechanism study of geopolymers prepared from ferronickel slag with high fire resistance, Constr. Build. Mater. 438 (Aug. 2024) 137282, https://doi.org/10.1016/J.CONBUILDMAT.2024.137282.

[14] Q. Van Nguyen, Y.S. Choi, Y.W. Jeong, S.Y. Han, S.K. Choi, Catalytic co-pyrolysis of coffee-grounds and waste polystyrene foam by calcium oxide in bubbling fluidized bed reactor, Renew. Energy 224 (2024), https://doi.org/10.1016/j.renene.2024.120124.

[15] M. Saberian, et al., Recycling of Spent Coffee Grounds in Construction Materials: A Review, 2021, https://doi.org/10.1016/j.jclepro.2021.125837.

[16] R. Saxena, H. Laddha, R.G. Bhoi, Sustainable Management of Spent Coffee Grounds: Applications, Decompositions Techniques and Structural Analysis, Springer, 2024, https://doi.org/10.1007/s10163-024-02113-3.

[17] M. Charai, O. Horma, A. El Hammouti, A. Mezrhab, M. Karkri, Thermophysical characteristics of cement-based mortar incorporating spent coffee grounds, Mater. Today Proc. 57 (2022), https://doi.org/10.1016/j.matpr.2022.02.488.

[18] A. Arulrajah, T.A. Kua, C. Suksiripattanapong, S. Horpibulsuk, J.S. Shen, Compressive strength and microstructural properties of spent coffee grounds-bagasse ash based geopolymers with slag supplements, J. Clean. Prod. 162 (2017), https://doi.org/10.1016/j.jclepro.2017.06.171.

[19] R. Roychand, S. Kilmartin-Lynch, M. Saberian, J. Li, G. Zhang, C.Q. Li, Transforming spent coffee grounds into a valuable resource for the enhancement of concrete strength, J. Clean. Prod. 419 (2023), https://doi.org/10.1016/j.jclepro.2023.138205.

[20] D.W. Cho, et al., Adsorption of potentially harmful elements by metal-biochar prepared via Co-pyrolysis of coffee grounds and Nano Fe(III) oxides, Chemosphere 319 (Apr. 2023) 136536, https://doi.org/10.1016/J.CHEMOSPHERE.2022.136536.

[21] E. Garcia, I.F. Ejim, H. Liu, Thermogravimetric analysis of co-combustion of a bituminous coal and coffee industry by-products, Thermochim. Acta 715 (Sep. 2022) 179296, https://doi.org/10.1016/J.TCA.2022.179296.

[22] G. Mohamed, B. Djamila, Properties of dune sand concrete containing coffee waste, MATEC Web of Conferences 149 (2018), https://doi.org/10.1051/matecconf/201814901039.

[23] S. Lawanwadeekul, A. Srisuwan, N. Phonphuak, P. Chindaprasirt, Addition of spent coffee grounds and waste glass to enhance the physical–mechanical and thermal properties of fired clay bricks at reduced temperatures, Innovative Infrastructure Solutions 9 (6) (Jun. 2024), https://doi.org/10.1007/s41062-024-01508-3.

[24] G. La Scalia, M. Saeli, P.P. Miglietta, R. Micale, Coffee biowaste valorization within circular economy: an evaluation method of spent coffee grounds potentials for

mortar production, Int. J. Life Cycle Assess. 26 (9) (2021), https://doi.org/10.1007/s11367-021-01968-0.
[25] M. Saeli, et al., Development of energy-saving innovative hydraulic mortars reusing spent coffee ground for applications in construction, J. Clean. Prod. 399 (May 2023) 136664, https://doi.org/10.1016/J.JCLEPRO.2023.136664.
[26] M. Saeli, V.S. Batra, R.K. Singh, D.M. Tobaldi, J.A. Labrincha, The coffee-house: upcycling spent coffee grounds for the production of green geopolymeric architectural energy-saving products, Energy Build. 286 (2023), https://doi.org/10.1016/j.enbuild.2023.112956.
[27] T.T. Le, S.S. Park, J.C. Lee, D.E. Lee, Strength characteristics of spent coffee grounds and oyster shells cemented with GGBS-based alkaline-activated materials, Constr. Build. Mater. 267 (2021), https://doi.org/10.1016/j.conbuildmat.2020.120986.
[28] Turkish Standards Institute. TS EN 196-1, Methods of Testing Cement - Part 1, Determination of strength, Ankara, 2016.
[29] R. Campos-Vega, G. Loarca-Piña, H.A. Vergara-Castañeda, B. Dave Oomah, Spent coffee grounds: a review on current research and future prospects, Trends Food Sci. Technol. 45 (1) (Sep. 2015) 24–36, https://doi.org/10.1016/J.TIFS.2015.04.012.
[30] F. Andreola, et al., Spent coffee grounds in the production of lightweight clay ceramic aggregates in view of urban and agricultural sustainable development, Materials 12 (21) (2019), https://doi.org/10.3390/ma12213581.
[31] R. Kohani Khoshkbijari, A. Farahmandfar, N. Zaati Zehni, M. Fard Samimi, Properties of ground granulated blast-furnace slag-based geopolymer mortars containing glass powder, feldspar, and metakaolin under different curing conditions, Constr. Build. Mater. 435 (Jul. 2024) 136753, https://doi.org/10.1016/J.CONBUILDMAT.2024.136753.
[32] S.D.C. Gomes, Q.D. Nguyen, W. Li, A. Castel, Carbonation resistance of calcined clay-ground granulated blast furnace slag alkali-activated mortar, Constr. Build. Mater. 393 (Aug. 2023) 131811, https://doi.org/10.1016/J.CONBUILDMAT.2023.131811.
[33] M.H. Nofalah, P. Ghadir, H. Hasanzadehshooiili, M. Aminpour, A.A. Javadi, M. Nazem, Effects of binder proportion and curing condition on the mechanical characteristics of volcanic ash- and slag-based geopolymer mortars; machine learning integrated experimental study, Constr. Build. Mater. 395 (Sep. 2023) 132330, https://doi.org/10.1016/J.CONBUILDMAT.2023.132330.
[34] M.U. Toprak, A.F. Şenol, C. Karakurt, Tuğla, kiremit ve mermer atığı tozları ile üretilen jeopolimer harçların özellikleri, Bilecik Şeyh Edebali Üniversitesi Fen Bilimleri Dergisi 9 (2) (2022), https://doi.org/10.35193/bseufbd.1100183.
[35] A. Sharmin, U.J. Alengaram, M.Z. Jumaat, M.O. Yusuf, S.M.A. Kabir, I.I. Bashar, Influence of source materials and the role of oxide composition on the performance of ternary blended sustainable geopolymer mortar, Constr. Build. Mater. 144 (Jul. 2017) 608–623, https://doi.org/10.1016/J.CONBUILDMAT.2017.03.178.
[36] Turkish Standards Institute. TS EN 12390-1, Testing Hardened Concrete - Part 1: Shape, Dimensions and Other Requirements for Specimens and Moulds, 2021. Ankara.
[37] Turkish Standards Institute. TS EN 1015-3, Methods of Test for Mortar for Masonry- Part 3: Determination of Consistence of Fresh Mortar (By Flow Table), 2006. Ankara.
[38] Turkish Standards Institute. TS EN 772-4, Methods of Test for Masonry Units - Part 4: Determination of Real and Bulk Density and of Total and Open Porosity for Natural Stone Masonry Units, 2000. Ankara.
[39] Turkish Standards Institute. TS EN 12504-4, Testing Concrete in Structures - Part 4: Determination of Ultrasonic Pulse Velocity, 2021. Ankara.
[40] Turkish Standards Institute. TS EN 1015-11, Methods of Test for Mortar for Masonry - Part 11: Determination of Flexural and Compressive Strength of Hardened Mortar, 2020. Ankara.
[41] E.H. Alakara, O. Sevim, I. Demir, O. Şimşek, Experimental study on firebrick powder-based cementitious composites under the effect of elevated temperature, J. Build. Eng. 61 (Dec. 2022) 105277, https://doi.org/10.1016/J.JOBE.2022.105277.
[42] T.B. Baştürk, A. Yılmaz, Y. Aygörmez, Sulfate attack, freeze-thaw and high-temperature performances by evaluation of colemanite waste as binding material and aggregate in green geopolymer production, Sustain Chem Pharm 43 (Feb. 2025) 101872, https://doi.org/10.1016/J.SCP.2024.101872.
[43] A. Raif Boğa, C. Karakurt, A. Ferdi Şenol, The effect of elevated temperature on the properties of SCC's produced with different types of fibers, Constr. Build. Mater. 340 (Jul. 2022) 127803, https://doi.org/10.1016/J.CONBUILDMAT.2022.127803.
[44] A. Arulrajah, T.A. Kua, S. Horpibulsuk, M. Mirzababaei, A. Chinkulkijniwat, Recycled glass as a supplementary filler material in spent coffee grounds geopolymers, Constr. Build. Mater. 151 (2017), https://doi.org/10.1016/j.conbuildmat.2017.06.050.
[45] P.J. Ardhira, S.K. Shukla, D. Sathyan, Synthesis of geopolymer mortar from biomass ashes and forecasting its compressive strength behaviour, Case Stud. Constr. Mater. 21 (Dec. 2024) e03581, https://doi.org/10.1016/J.CSCM.2024.E03581.
[46] A.K. Farag Gaddafi, U.J. Alengaram, N.M. Bunnori, M.S.I. Ibrahim, S. Ibrahim, S. Govindasami, Enhancement of ductility characteristics of fiber-reinforced ternary geopolymer mortar, J. Build. Eng. 82 (2024), https://doi.org/10.1016/j.jobe.2023.108141.
[47] S. Park, M. Pour-Ghaz, What is the role of water in the geopolymerization of metakaolin? Constr. Build. Mater. 182 (2018) https://doi.org/10.1016/j.conbuildmat.2018.06.073.
[48] W. Wang, C. Fan, B. Wang, X. Zhang, Z. Liu, Workability, rheology, and geopolymerization of fly ash geopolymer: role of alkali content, modulus, and water–binder ratio, Constr. Build. Mater. 367 (Feb. 2023) 130357, https://doi.org/10.1016/J.CONBUILDMAT.2023.130357.
[49] O.A. Abdulkareem, A.M. Mustafa Al Bakri, H. Kamarudin, I. Khairul Nizar, A. A. Saif, Effects of elevated temperatures on the thermal behavior and mechanical performance of fly ash geopolymer paste, mortar and lightweight concrete, Constr. Build. Mater. 50 (Jan. 2014) 377–387, https://doi.org/10.1016/J.CONBUILDMAT.2013.09.047.
[50] B. Bayrak, et al., Effects of silica fume and rice husk ash contents on engineering properties and high-temperature resistance of slag-based prepacked geopolymers, J. Build. Eng. 92 (Sep. 2024) 109746, https://doi.org/10.1016/J.JOBE.2024.109746.
[51] A. Sedaghatdoost, K. Behfarnia, M. Bayati, M. sadegh Vaezi, Influence of recycled concrete aggregates on alkali-activated slag mortar exposed to elevated temperatures, J. Build. Eng. 26 (Nov. 2019) 100871, https://doi.org/10.1016/J.JOBE.2019.100871.
[52] A. Saludung, T. Azeyanagi, Y. Ogawa, K. Kawai, Mechanical and microstructural evolutions of fly ash/slag-based geopolymer at high temperatures: effect of curing conditions, Ceram. Int. 49 (2) (2023), https://doi.org/10.1016/j.ceramint.2022.09.175.
[53] E. Annerel, L. Taerwe, Methods to quantify the colour development of concrete exposed to fire, Constr. Build. Mater. 25 (10) (Oct. 2011) 3989–3997, https://doi.org/10.1016/J.CONBUILDMAT.2011.04.033.
[54] E.D. Shumuye, J. Zhao, Z. Wang, Effect of the curing condition and high-temperature exposure on ground-granulated blast-furnace slag cement concrete, Int J Concr Struct Mater 15 (1) (2021), https://doi.org/10.1186/s40069-020-00437-6.
[55] M. Dudek, M. Sitarz, Analysis of changes in the microstructure of geopolymer mortar after exposure to high temperatures, Materials 13 (19) (2020), https://doi.org/10.3390/MA13194263.
[56] I. Hager, M. Sitarz, K. Mróz, Fly-ash based geopolymer mortar for high-temperature application – effect of slag addition, J. Clean. Prod. 316 (2021), https://doi.org/10.1016/j.jclepro.2021.128168.
[57] G. Kaplan, J. Shi, A. Öz, B. Bayrak, M.H. Dheyaaldin, A.C. Aydın, Preparation and characterization of a novel prepacked aggregate geopolymer: a feasibility study, Powder Technol. 421 (2023), https://doi.org/10.1016/j.powtec.2023.118423.
[58] Z. Funda Akbulut, S. Guler, M. Khan, The effects of waste iron powder and steel fiber on the physical and mechanical properties of geopolymer mortars exposed to high temperatures, Structures 58 (2023), https://doi.org/10.1016/j.istruc.2023.105398.
[59] A.F. Şenol, C. Karakurt, High-strength self-compacting concrete produced with recycled clay brick powders: rheological, mechanical and microstructural properties, J. Build. Eng. 88 (Jul. 2024) 109175, https://doi.org/10.1016/J.JOBE.2024.109175.
[60] M.M. Jibril, et al., Implementation of nonlinear computing models and classical regression for predicting compressive strength of high-performance concrete, Applications in Engineering Science 15 (2023), https://doi.org/10.1016/j.apples.2023.100133.
[61] P. Zhang, Y. Mao, W. Yuan, J. Zheng, S. Hu, K. Wang, A critical review on modeling and prediction on properties of fresh and hardened geopolymer composites, J. Build. Eng. 88 (Jul. 2024) 109184, https://doi.org/10.1016/J.JOBE.2024.109184.
[62] M. Naveed, A. Hameed, M.U. Qureshi, A.M. Rasool, Optimization of constituent proportions for compressive strength of sustainable geopolymer concrete: a statistical approach, Results in Engineering 20 (2023), https://doi.org/10.1016/j.rineng.2023.101575.
[63] S. Janga, A.N. Raut, M. Adamu, Y.E. Ibrahim, Thermo-mechanical performance assessment of geopolymer synthesized with steel slag and glass powder at elevated temperatures, Powder Technol. 444 (Aug. 2024) 120047, https://doi.org/10.1016/J.POWTEC.2024.120047.
[64] J.L. Provis, Geopolymers and other alkali activated materials: why, how, and what? Materials and Structures/Materiaux et Constructions 47 (2014) 1–2, https://doi.org/10.1617/s11527-013-0211-5.
[65] D.K. Ashish, Feasibility of waste marble powder in concrete as partial substitution of cement and sand amalgam for sustainable growth, J. Build. Eng. 15 (Jan. 2018) 236–242, https://doi.org/10.1016/J.JOBE.2017.11.024.
[66] F. Jia, L. Chen, J. Zhang, Q. Hu, Y. Wang, Effect of sodium stearate modified waste marble powder on the properties and hydration of cement mortar, Constr. Build. Mater. 465 (Feb. 2025) 140213, https://doi.org/10.1016/J.CONBUILDMAT.2025.140213.
[67] A.A. Aliabdo, A.E.M. Abd Elmoaty, E.M. Auda, Re-use of waste marble dust in the production of cement and concrete, Constr. Build. Mater. 50 (Jan. 2014) 28–41, https://doi.org/10.1016/J.CONBUILDMAT.2013.09.005.
[68] B.S. Almada, et al., Influence of the heterogeneity of waste from wet processing of ornamental stones on the performance of Portland cement composites, Constr. Build. Mater. 262 (Nov. 2020) 120036, https://doi.org/10.1016/J.CONBUILDMAT.2020.120036.
[69] Y. Shin, et al., Utilization of artificial interior stone sludge as fine aggregate in controlled low-strength material (CLSM), J. Build. Eng. 71 (Jul. 2023) 106441, https://doi.org/10.1016/J.JOBE.2023.106441.
[70] K. Eryılmaz, R. Polat, Sustainable concrete production: mechanical and durability behaviour of slag-based geopolymer containing recycled geopolymer aggregate, J. Build. Eng. 96 (Nov. 2024) 110512, https://doi.org/10.1016/J.JOBE.2024.110512.
[71] S. Saha, C. Rajasekaran, Enhancement of the properties of fly ash based geopolymer paste by incorporating ground granulated blast furnace slag, Constr.

Build. Mater. 146 (Aug. 2017) 615–620, https://doi.org/10.1016/J.CONBUILDMAT.2017.04.139.
[72] Y. Hu, Z. Jin, B. Pang, Y. Huang, H. Sun, Z. Du, Effect of high-activity MgO on drying shrinkage and microstructure of geopolymer coatings, J. Build. Eng. 102 (May 2025) 111972, https://doi.org/10.1016/J.JOBE.2025.111972.
[73] S.A. Bernal, et al., MgO content of slag controls phase evolution and structural changes induced by accelerated carbonation in alkali-activated binders, Cement Concr. Res. 57 (Mar. 2014) 33–43, https://doi.org/10.1016/J.CEMCONRES.2013.12.003.